J|A|C|S
ARTICLES
Published on Web 02/17/2004

Promotion of Iridium-Catalyzed Methanol Carbonylation: Mechanistic Studies of the Cativa Process

Anthony Haynes,*,† Peter M. Maitlis,*,† George E. Morris,*,‡ Glenn J. Sunley,*,‡ Harry Adams,† Peter W. Badger,† Craig M. Bowers,† David B. Cook,† Paul I. P. Elliott,† Talit Ghaffar,† Helena Green,† Tim R. Griffin,† Marc Payne,‡ Jean M. Pearson,† Michael J. Taylor,§ Paul W. Vickers,† and Rob J. Watt‡

Contribution from the Department of Chemistry, University of Sheffield, Sheffield, S3 7HF, U.K., BP Chemicals Ltd, Hull Research and Technology Centre, Saltend, Hull, HU12 8DS, U.K., and BP Chemicals Ltd, Chertsey Road, Sunbury-on-Thames, Middlesex, TW16 7LL, U.K.

Received November 6, 2003; E-mail: a.haynes@sheffield.ac.uk; sunleyg@bp.com

Abstract: The iridium/iodide-catalyzed carbonylation of methanol to acetic acid is promoted by carbonyl complexes of W, Re, Ru, and Os and simple iodides of Zn, Cd, Hg, Ga, and In. Iodide salts (LiI and Bu_4NI) are catalyst poisons. In situ IR spectroscopy shows that the catalyst resting state (at H_2O levels $\geq$ 5% w/w) is *fac,cis*-$[Ir(CO)_2I_3Me]^-$, **2**. The stoichiometric carbonylation of **2** into $[Ir(CO)_2I_3(COMe)]^-$, **6**, is accelerated by substoichiometric amounts of neutral promoter species (e.g., $[Ru(CO)_3I_2]_2$, $[Ru(CO)_2I_2]_n$, InI_3, GaI_3, and ZnI_2). The rate increase is approximately proportional to promoter concentration for promoter:Ir ratios of 0−0.2. By contrast anionic Ru complexes (e.g., $[Ru(CO)_3I_3]^-$, $[Ru(CO)_2I_4]^{2-}$) do not promote carbonylation of **2** and Bu_4NI is an inhibitor. Mechanistic studies indicate that the promoters accelerate carbonylation of **2** by abstracting an iodide ligand from the Ir center, allowing coordination of CO to give $[Ir(CO)_3I_2Me]$, **4**, identified by high-pressure IR and NMR spectroscopy. Migratory CO insertion is ca. 700 times faster for **4** than for **2** (85 °C, PhCl), representing a lowering of $\Delta G^{\ddagger}$ by 20 kJ mol^{-1}. Ab initio calculations support a more facile methyl migration in **4**, the principal factor being decreased π-back-donation to the carbonyl ligands compared to **2**. The *fac,cis* isomer of $[Ir(CO)_2I_3(COMe)]^-$, **6a** (as its Ph_4As^+ salt), was characterized by X-ray crystallography. A catalytic mechanism is proposed in which the promoter $[M(CO)_mI_n]$ (M = Ru, In; m = 3, 0; n = 2, 3) binds I^- to form $[M(CO)_mI_{n+1}]^-H_3O^+$ and catalyzes the reaction $HI_{(aq)}$ + MeOAc → MeI + HOAc. This moderates the concentration of $HI_{(aq)}$ and so facilitates catalytic turnover via neutral **4**.

Introduction

One of the most successful industrial applications of homogeneous transition metal catalysis is the carbonylation of methanol to acetic acid.[1] The global annual manufacturing capacity for acetic acid is ca. 8 million tonnes, about 80% of which is based on methanol carbonylation technology. In the last 40 years, there have been three major advances in the catalyst system used commercially, descending group 9 of the periodic table from cobalt[2] to rhodium[3,4] and, most recently, iridium. The rhodium-based process was the basis of most new acetic acid manufacturing capacity after its commercialization by Monsanto in 1970. In 1996, BP Chemicals announced a new methanol carbonylation process, Cativa,[5] based upon a promoted iridium/iodide catalyst, which now operates on four plants worldwide. Promoters, which enhance the catalytic activity, are key to the success of the iridium-based process.[6] In this paper, we combine the results of catalytic studies with mechanistic and theoretical investigations of key steps in the catalytic cycle, to identify the mechanism by which the promoters act.

The Cativa Process. The key features of the Cativa process have been reported elsewhere[7−10] and will be summarized here to place the mechanistic studies in context. A broad range of conditions are accessible for the Ir catalyst without precipitation of IrI_3 occurring.[11] By contrast, the precipitation of RhI_3 at low pCO can be problematic in the product purification stage of

† University of Sheffield.
‡ BP Chemicals Ltd, Hull Research and Technology Centre.
§ BP Chemicals Ltd, Sunbury-on-Thames.

(1) Howard, M. J.; Jones, M. D.; Roberts, M. S.; Taylor, S. A. *Catal. Today* **1993**, *18*, 325. Yoneda, N.; Kusano, S.; Yasui, M.; Pujado, P.; Wilcher, S. *Appl. Catal. A* **2001**, *221*, 253.
(2) Hohenschutz, H.; von Kutepow, N.; Himmle, W. *Hydrocarbon Process* **1966**, *45*, 141. von Kutepow, N.; Himmle, W.; Hohenschutz, H. *Chem.-Ing.-Tech.* **1966**, *37*, 383.
(3) Paulik, F. E.; Roth, J. F. *Chem. Commun.* **1968**, 1578.
(4) Roth, J. F.; Craddock, J. H.; Hershman, A.; Paulik, F. E. *Chemtech* **1971**, 600. Eby, R. T.; Singleton, T. C. *Appl. Ind. Catal.* **1971**, 483.
(5) *Chem. Br.* **1996**, *32*, 7. *Chem. Ind. (London)* **1996**, 483.
(6) Garland, C. S.; Giles, M. F.; Sunley, J. G. Eur. Pat. Pub. 0643034, 1995. Garland, C. S.; Giles, M. F.; Poole, A. D.; Sunley, J. G. Eur. Pat. Pub. 0728726, 1996. Baker, M. J.; Giles, M. F.; Garland, C. S.; Rafeletos, G. Eur. Pat. Pub. 0749948, 1996. Baker, M. J.; Giles, M. F.; Garland, C. S.; Muskett, M. J.; Rafeletos, G.; Smith, S. J.; Sunley, J. G.; Watt, R. J.; Williams, B. L. Eur. Pat. Pub. 0752406, 1997.
(7) Howard, M. J.; Sunley, G. J.; Poole, A. D.; Watt, R. J.; Sharma, B. K. *Stud. Surf. Sci. Catal.* **1999**, *121*, 61.
(8) Sunley, G. J.; Watson, D. J. *Catal. Today* **2000**, *58*, 293.
(9) Jones, J. H. *Platinum Metals Rev.* **2000**, *44*, 94.
(10) Haynes, A. *Educ. Chem.* **2001**, *38*, 99.
(11) Clode, K. E.; Watson, D. J.; Vercauteren, C. J. E. Eur. Pat. Pub. 0616997, 1994. Clode, K. E. Eur. Pat. Pub. 0786447, 1997.

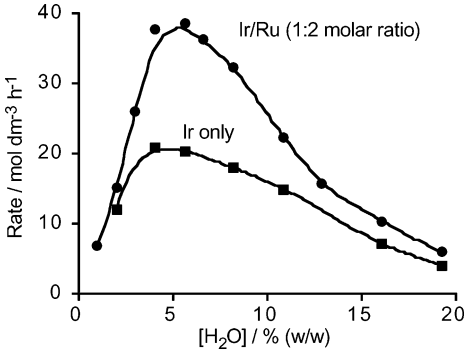

Figure 1. Batch autoclave data[8] for iridium and iridium/ruthenium catalysts: effect of water concentration on carbonylation rate at ca. 30% (w/w) MeOAc, 8.4% (w/w) MeI, 1950 ppm Ir, 28 barg total pressure, and 190 °C. The data plotted are listed in the Supporting Information (Table S1).

the Rh-based process. The greater stability of the iridium catalyst can be ascribed to stronger metal−ligand bonding for the third-row metal, which inhibits CO loss from the Ir center.

The rate of iridium-catalyzed carbonylation displays a rather complicated dependence on a range of process variables such as *p*CO, [MeI], [MeOAc], and [H_2O]. The catalytic rate displays a strong positive dependence on [MeOAc] but is zero order in [MeI] above a limiting threshold and independent of CO partial pressure above ca. 10 bar. Figure 1 illustrates a rate profile with respect to [H_2O] which shows that maximum activity is achieved at ca. 5% w/w H_2O.[12]

A range of compounds can enhance the activity of the iridium catalyst. The promoters fall into two categories: (i) carbonyl or halocarbonyl complexes of W, Re, Ru, and Os; (ii) simple iodides of Zn, Cd, Hg, Ga, and In. None of the promoters show any detectable activity in the absence of iridium catalyst, although ruthenium has been reported previously to catalyze methanol carbonylation, albeit under harsh conditions and with relatively low selectivity.[13] For a promoter:Ir mole ratio of 5:1 the carbonylation rate is enhanced by factors of 2.6 ([$Ru(CO)_4I_2$]); 2.3 ([$Os(CO)_4I_2$]); 1.2 ([$Re(CO)_5Cl$]); 1.1 ([$W(CO)]_6$); 1.4 (ZnI_2, HgI_2); 1.8 (CdI_2); 1.5 (GaI_3); and 1.8 (InI_3) (Supporting Information Table S2). A ruthenium promoter (added as [$Ru(CO)_4I_2$]) is effective over a range of water concentrations (Figure 1). By contrast, ionic iodides such as LiI and Bu_4NI are both strong catalyst *poisons*, reducing activity by factors of ca. 2 and 3, respectively, when added in a 1:1 molar ratio with Ir.

Mechanism of Iridium-Catalyzed Methanol Carbonylation. Iridium/iodide catalysts for the carbonylation of methanol were first identified by Monsanto,[3] and elegant mechanistic studies were reported by Forster.[14] Others have also investigated iridium-based catalysts.[15,16] The catalytic cycle is thought to involve fundamental steps similar to those in the well-established rhodium system:[17] oxidative addition of MeI to Ir(I), followed by migratory CO insertion to form an acetyl complex which is the precursor to acetic acid. On the basis of spectroscopic and kinetic observations, Forster proposed that two different (but linked) cycles exist,[14] one involving neutral iridium complexes, and the other predominantly anionic species (Scheme 1). Similar neutral and anionic cycles were also proposed for the competing water gas shift reaction. At low concentrations of water and iodide, the "neutral cycle" operated, with [$Ir(CO)_3I$] (**9**) as the resting state and rate-determining oxidative addition of MeI to [$Ir(CO)_2I$] (**8**). At higher iodide concentrations the "anionic cycle" predominated, and the catalyst resting state was *fac,cis*-[$Ir(CO)_2I_3Me]^-$ (**2**). Under these conditions, the rate of catalysis increased with CO pressure but was inhibited by ionic iodide. It was proposed that the rate-determining step involves dissociative substitution of I^- by CO in **2**, followed by migratory CO insertion in the tricarbonyl **4**. This contrasts with the rhodium sytem, in which oxidative addition of MeI to [$Rh(CO)_2I_2]^-$ is rate determining. Model kinetic studies[18,19] have shown that addition of MeI to [$Ir(CO)_2I_2]^-$ (**1**) is much faster (ca. 100 times) than to the rhodium analogue.

We have communicated preliminary data concerning the reactivity of the anionic iridium methyl species **2** and the first detection of neutral **4**.[20,21] In this paper we present the results of in situ spectroscopic, kinetic, mechanistic, and theoretical studies aimed at determining the mechanism by which promoters enhance the activity of an iridium catalyst. Our results show that a key feature of all the promoters is their ability to accept an iodide ion and facilitate conversion of **2** into **4**, which undergoes substantially faster migratory insertion.

Results and Discussion

Batch Autoclave Catalytic Reactions. In addition to the data summarized in the Introduction, further studies have been performed to determine how the catalytic rate depends on process variables and additives. In batch autoclave tests methyl acetate is used as the substrate, together with water at an appropriate concentration. This mimics the process conditions in which the standing concentration of methanol is low due to esterification by the acetic acid cosolvent. The overall reaction occurring in these batch studies can therefore be represented as

$$\mathrm{MeOAc} + \mathrm{CO} + \mathrm{H_2O} \rightarrow 2\ \mathrm{AcOH} \qquad (1)$$

Figure 2 compares the effects of Ru and In promoters with the effect of LiI over a range of additive:Ir ratios. The carbonylation rate is strongly inhibited at high concentrations of ionic iodide, but the effect can be partially suppressed by increasing the CO pressure. Notably, the promotional effect of

(12) The water concentration at which the maximum rate is attained varies with [MeOAc], [MeI], and [CO].
(13) Jenner, G.; Bitsi, G. *J. Mol. Catal.* **1987**, *40*, 71. Kelkar, A. A.; Kohle, D. S.; Chaudhari, R. V. *J. Organomet. Chem.* **1992**, *430*, 111. Braca, G.; Paladini, L.; Sbrana, G.; Valentini, G.; Andrich, G.; Gregorio, G. *Ind. Eng. Chem. Prod. Res. Dev.* **1981**, *20*, 115. Braca, G.; Sbrana, G.; Valentini, G.; Andrich, G.; Gregorio, G. *J. Am. Chem. Soc.* **1978**, *100*, 6238. Braca, G.; Sbrana, G.; Valentini, G.; Cini, M. *J. Mol. Catal.* **1982**, *17*, 323. Gautier-Lafaye, J.; Perron, R.; Leconte, P.; Colleuille, Y. *Bull. Soc. Chim. Fr.* **1985**, 353.
(14) Forster, D. *J. Chem. Soc., Dalton Trans.* **1979**, 1639.
(15) Brodzki, D.; Denise, B.; Pannetier, G. *J. Mol. Catal.* **1977**, *2*, 149. Mizoroki, T.; Matsumoto, T.; Ozaki, A. *Bull. Chem. Soc. Jpn.* **1979**, *52*, 479.
(16) Matsumoto, T.; Mizoroki, T.; Ozaki, A. *J. Catal.* **1978**, *51*, 96.
(17) Forster, D.; Singleton, T. C. *J. Mol. Catal.* **1982**, *17*, 299. Forster, D. *Adv. Organomet. Chem.* **1979**, *17*, 255. Maitlis, P. M.; Haynes, A.; Sunley, G. J.; Howard, M. J. *J. Chem. Soc., Dalton Trans.* **1996**, 2187. Haynes, A.; Mann, B. E.; Gulliver, D. J.; Morris, G. E.; Maitlis, P. M. *J. Am. Chem. Soc.* **1991**, *113*, 8567. Haynes, A.; Mann, B. E.; Morris, G. E.; Maitlis, P. M. *J. Am. Chem. Soc.* **1993**, *115*, 4093.
(18) Bassetti, M.; Monti, D.; Haynes, A.; Pearson, J. M.; Stanbridge, I. A.; Maitlis, P. M. *Gazz. Chim. Ital.* **1992**, *122*, 391.
(19) Ellis, P. R.; Pearson, J. M.; Haynes, A.; Adams, H.; Bailey, N. A.; Maitlis, P. M. *Organometallics* **1994**, *13*, 3215.
(20) Pearson, J. M.; Haynes, A.; Morris, G. E.; Sunley, G. J.; Maitlis, P. M. *J. Chem. Soc., Chem. Commun.* **1995**, 1045.
(21) Ghaffar, T.; Adams, H.; Maitlis, P. M.; Sunley, G. J.; Baker, M. J.; Haynes, A. *Chem. Commun.* **1998**, 1023.

Scheme 1. Anionic and Neutral Cycles Proposed by Forster for Iridium-Catalyzed Methanol Carbonylation (adapted from Ref 14)

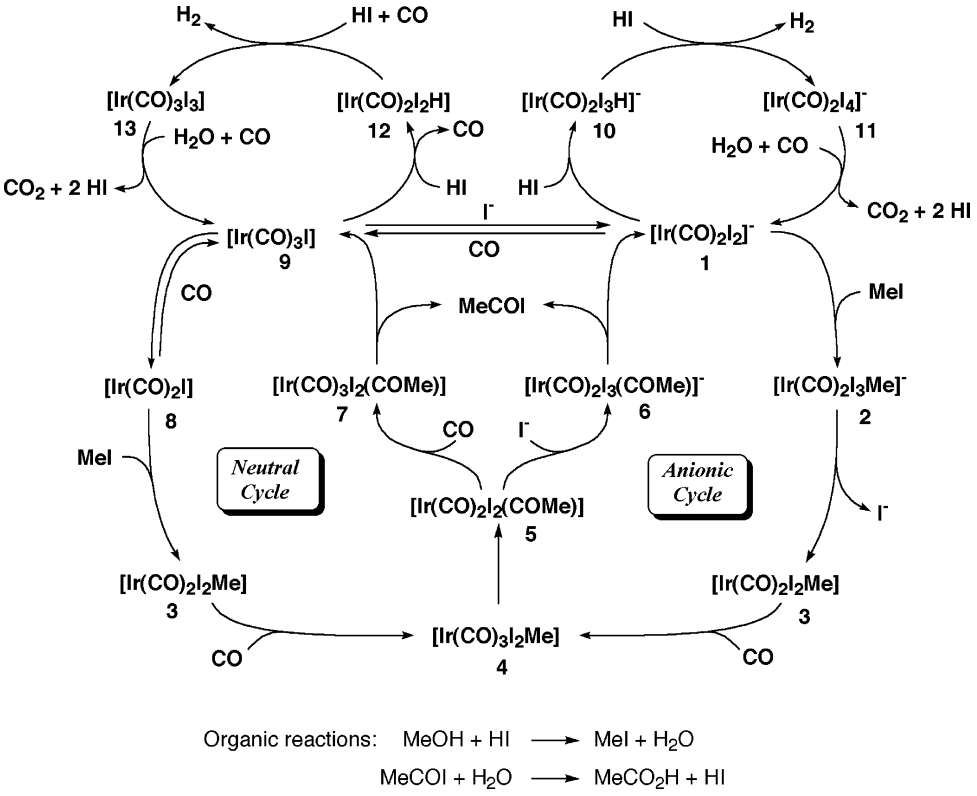

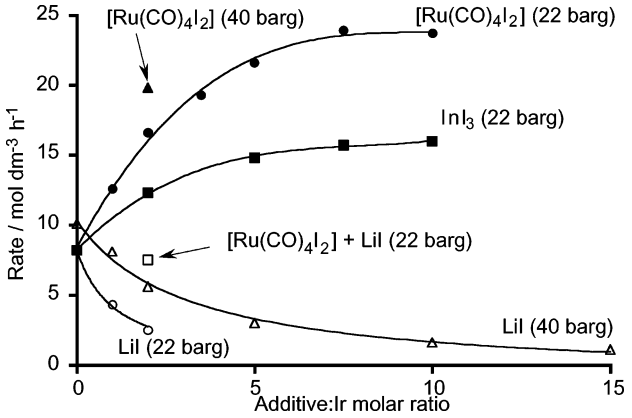

Figure 2. Batch autoclave data: effect of $[Ru(CO)_4I_2]$, InI_3, and LiI on carbonylation rate (190 °C, 1500 rpm). Total pressures 22 and 40 barg correspond to CO partial pressures 7.5 and 25.5 bar, respectively. Autoclave charge: MeOAc (648 mmol), H_2O (943 mmol), AcOH (1258 mmol), MeI (62 mmol), H_2IrCl_6 (1.56 mmol) plus additive if required. Carbonylation rate measured at 50% conversion of MeOAc.

$[Ru(CO)_4I_2]$ (Ru:Ir = 2:1) is removed when an equimolar quantity of LiI is also added (equivalent to addition of $Li[Ru(CO)_3I_3]$). A corollary of this is that the inhibiting effect of LiI is negated by the addition of an equimolar amount of $[Ru(CO)_4I_2]$.

The effect of a ruthenium promoter was also examined over the range 170−200 °C (Supporting Information Table S3). Eyring plots of the data gave the apparent activation parameters listed in Table 1. Addition of a ruthenium promoter has a rather subtle effect, with a slightly higher $\Delta H^{\ddagger}$ being offset by a less negative $\Delta S^{\ddagger}$, resulting in a lowering of $\Delta G^{\ddagger}$(190 °C) by less than 2 kJ mol^{-1}. The Ir and Ir/Ru catalysts exhibit larger $\Delta H^{\ddagger}$ but less negative values of $\Delta S^{\ddagger}$ than those for Rh catalysts,[22] consistent with a different rate equation.

In Situ Spectroscopic Studies of Catalyst Species. The metal carbonyl complexes present during batch catalytic reactions were probed in situ using high-pressure infrared (HPIR) spectroscopy. Selected spectra are provided in the Supporting Information (Figures S1−S4). In the absence of additives the catalyst precursor, H_2IrCl_6, was rapidly converted into iridium iodocarbonyl species after injection into the reaction solution, which had been allowed to reach the required temperature and pressure (190 °C, 22 barg). For reactions conducted at relatively high $[H_2O]$ (i.e. ≥ ca. 5% w/w), the predominant (>95%) iridium species was the anionic methyl complex **2** (ν(CO) 2100, 2047 cm^{-1}), which can be regarded as the "active" form of the catalyst. A weak band at 1975 cm^{-1} indicated the presence of a small amount of $[Ir(CO)_2I_2]^-$, **1**. As the catalytic reaction proceeded, the concentration of **2** decreased and ν(CO) bands appeared at 2112 and 2065 cm^{-1}, characteristic of *cis*-$[Ir(CO)_2I_4]^-$ (**11**), which is regarded as an "inactive" catalyst. At 50% methyl acetate conversion, the ratio of "active" **2** to "inactive" **11** was approximately 1:1. The buildup of **11** as the reaction proceeds is caused by the decrease in water concentration according to eq 1, which lowers the rate of reduction of **11** to **1** in the water gas shift cycle. For reactions conducted at very low water concentrations ((i.e., $[H_2O]$ < ca. 4% w/w), bands due to $[Ir(CO)_3I]$ (**9**) (2070, 2049sh cm^{-1}) and $[Ir(CO)_3I_3]$ (**13**) (2186w, 2132 cm^{-1}) were observed,[7] consistent with the operation of the "neutral cycle" under these conditions. During reactions conducted in the presence of LiI or Bu_4NI (equimolar with Ir) infrared spectroscopy shows the catalyst to remain predominantly (≥90%) as the "active" species **2** at 50% MeOAc conversion, with buildup of **11** occurring only later in the

(22) Dekleva, T. W.; Forster, D. *Adv. Catal.* **1986**, *34*, 81. Smith, B. L.; Torrence, G. P.; Murphy, M. A.; Aguiló, A. *J. Mol. Catal.* **1987**, *39*, 115. Hjortkjaer, J.; Jensen, V. W. *Ind. Eng. Chem., Prod. Res. Dev.* **1976**, *15*, 46.

Table 1. Activation Parameters Derived from Eyring Plots of Kinetic Data Measured for Ir-Catalyzed Carbonylation and Stoichiometric Carbonylation of Iridium Methyl Complexes **2** and **4**

reaction	promoter (promoter:Ir)	solvent	$\Delta H^{\ddagger}$/kJ mol^{-1}	$\Delta S^{\ddagger}$/J mol^{-1} K^{-1}
Ir-catalyzed carbonylation[a]		AcOH	83 (±6)	−73 (±12)
Ir-catalyzed carbonylation[a]	Ru (2:1)	AcOH	96 (±3)	−40 (±6)
Ir-catalyzed carbonylation[16]		33% MeOH/PhCOMe	34 (±2)	−195 (±4)[b]
2 + CO → **6a** + **6b**		PhCl	152 (±6)	82 (±17)
2 + CO → **6a**		25% MeOH/PhCl	33 (±2)	−197 (±8)
2 + CO → **6a** + **6b**	Ru (1:13)	PhCl	90 (±5)	−63 (±12)
2 + CO → **6a** + **6b**	InI_3 (1:10)	PhCl	104 (±10)	−19 (±28)
2 + CO → **6a** + **6b**	**3d** (1:10)	PhCl	108 (±9)	−8 (±24)
4 + CO → **7**		PhCl	89 (±3)	−36 (±8)
4 + CO → **7**		1% MeOH/PhCl	73 (±2)	−79 (±6)

[a] Conditions as in Figure 2 with 40 barg total pressure. [b] Value of −246 J mol^{-1} K^{-1} given in ref 20 was wrongly calculated from the data in ref 16.

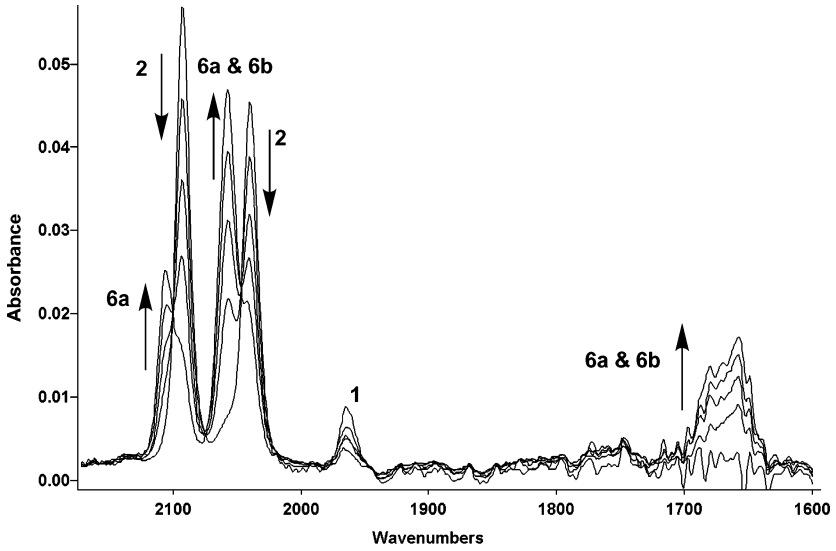

Figure 3. Series of in situ HPIR spectra for the reaction of **2** with CO (5.5 barg) in PhCl at 93 °C.

reaction. Thus iodide salts appear to lower the activity of **2** rather than convert it into an inactive iridium complex.

Prior to injection of the iridium catalyst, a ruthenium promoter (added as $[Ru(CO)_4I_2]$) was present (at 19 barg and 190 °C) as a mixture of ruthenium(II) iodocarbonyl species $[Ru(CO)_2I_2(sol)_2]$ (ν(CO) 2053, 1996 cm^{-1}), $[Ru(CO)_3I_2(sol)]$ (2126, 2068, 2012 cm^{-1}), and $[Ru(CO)_3I_3]^-$ (2107, 2041(sh) cm^{-1}). After injection of the iridium catalyst (with the conditions given in Figure 2, and Ru:Ir = 2:1), $[Ru(CO)_3I_3]^-$ became the dominant ruthenium species. At higher ruthenium concentrations (e.g., Ru:Ir = 10:1) the IR band intensities indicated a greater proportion of neutral ruthenium complexes (both before and after injection of the iridium catalyst). The strong ν(CO) bands of ruthenium carbonyl complexes hinder the observation of iridium species. However, in situ HPIR studies for an indium-promoted catalyst (InI_3:Ir 2:1) showed iridium speciation very similar to that observed in the absence of promoter, with **2** being converted into **11** as the reaction progressed.[23]

Model Reaction Studies: Carbonylation of 2. The reaction of **2** with CO (eq 2) was identified in Forster's original study[14] as the rate-determining step in the anionic cycle for catalytic carbonylation.

$$[Ir(CO)_2I_3Me]^- (\mathbf{2}) + CO \rightarrow [Ir(CO)_2I_3(COMe)]^- (\mathbf{6}) \quad (2)$$

In situ HPIR and HPNMR spectroscopy show that in weakly polar aprotic solvents the reaction proceeds slowly even at elevated temperatures (>80 °C). A typical set of IR spectra obtained for the reaction in PhCl is shown in Figure 3. The two ν(CO) bands of **2** at 2093 and 2040 cm^{-1} decay and are replaced by new absorptions due to **6** at 2105 (m), 2057 (s), and 1670 (m, br) cm^{-1}. An additional weak absorption at 1966 cm^{-1} is assigned to a small amount of **1**, presumably formed by reductive elimination of MeI from **2**.

^{1}H and ^{13}C HPNMR spectra for the reaction of $[Ir(^{13}CO)_2I_3(^{13}CH_3)]^-$ with ^{13}CO (42 barg) in CD_2Cl_2 at 80 °C revealed the slow formation of two isomers of $[Ir(^{13}CO)_2I_3(^{13}CO^{13}CH_3)]^-$ in a ca. 1:1 ratio.[24] The observed chemical shifts and coupling constants are listed in the Supporting Information (Table S8). A singlet for each isomer in the terminal CO region indicates equivalent CO ligands, and the absence of coupling between terminal and acetyl carbonyl resonances shows that neither isomer of **6** has acetyl *trans* to CO. The two isomers are therefore assigned as the *fac*,*cis* and *mer*,*trans* complexes, **6a** and **6b** (Scheme 2).[25] The unusual relative intensities of product ν(CO) bands in the IR (Figure 3) are explained by the

(23) An additional band at 2053 cm^{-1} is tentatively assigned to a *trans* dicarbonyl isomer of **2**. The intensity of this band was higher when the In:Ir ratio was increased from 2:1 to 10:1.

(24) Additional Ir methyl and acetyl species observed on prolonged heating are assigned as mixed halide species formed by halide exchange with the solvent. The Ir-Me species were assigned on the basis of exchange experiments using Bu_4NCl (Vickers, P. W. Ph.D. Thesis, University of Sheffield, 1997) as $[Ir(CO)_2Cl_2IMe]^-$ (Me *trans* to I) δ ^{13}C −2.91, 157.9, δ ^{1}H 1.71, $^1J_{H-C}$ 139 Hz; $[Ir(CO)_2Cl_2IMe]^-$ (Me *cis* to I) δ ^{13}C −9.30, 155.2, 158.7, δ ^{1}H 1.94, $^1J_{H-C}$ 139 Hz. The two acetyl species have δ ^{13}C 198.3, 196.3, 43.6, 39.4, $^1J_{C-C}$ 33 Hz in each case; δ ^{1}H 2.74, $^1J_{H-C}$ 130 Hz, $^2J_{H-C}$ 6 Hz, 2.67, $^1J_{H-C}$ 123 Hz, $^2J_{H-C}$ 7 Hz.

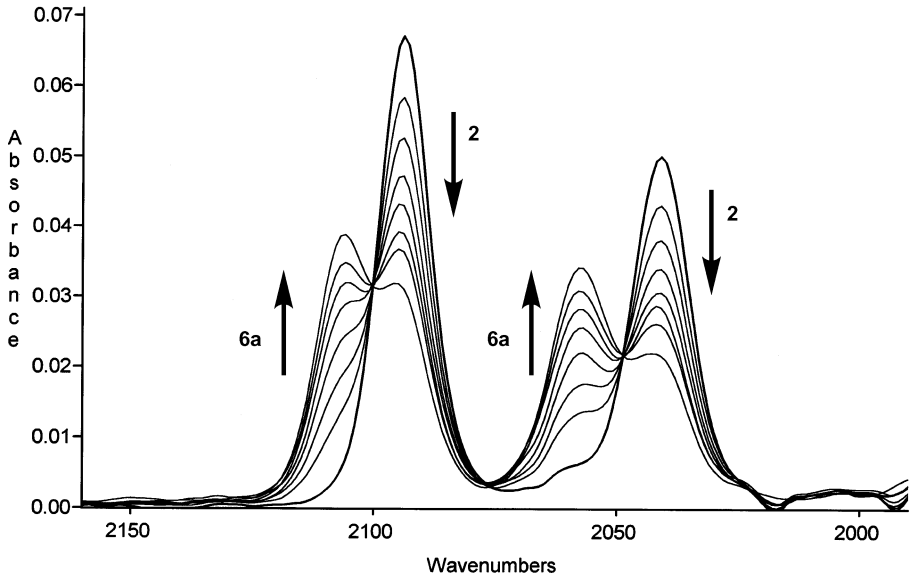

Figure 4. Series of IR spectra recorded in situ during the reaction of **2** with CO (5.5 barg) in PhCl−MeOH (3:1 v/v) at 33 °C.

Scheme 2. Proposed Mechanism for Carbonylation of **2** to Give **6a** and **6b**

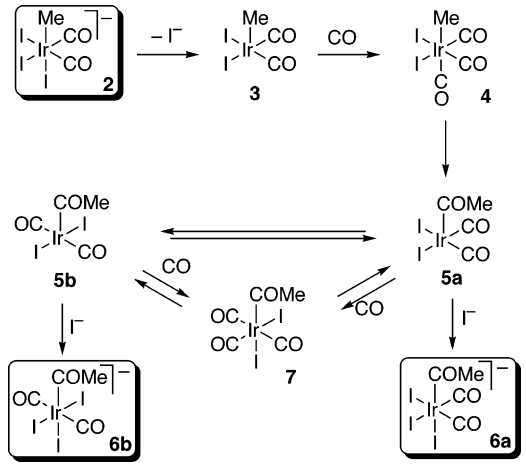

coincidence of the low-frequency antisymmetric ν(CO) modes of **6a** and **6b** at 2057 cm^{-1}.[26]

Carbonylation of **2** was much more facile on addition of methanol, and convenient reaction times were accessible at much lower temperatures (ca. 30−50 °C). A typical set of IR spectra for the reaction in PhCl−MeOH is shown in Figure 4. In this case, the two terminal ν(CO) bands of the product have similar intensities, indicating selective formation of the *fac*,*cis* isomer **6a**. At the high end of the temperature range employed, a band was also observed to grow at 1746 cm^{-1}, due to formation of MeOAc by methanolysis of **6a**.

In situ HPNMR spectroscopy showed that the reaction of $[Ir(^{13}CO)_2I_3(^{13}CH_3)]^-$ with ^{13}CO (6.3 barg) in CD_2Cl_2−CD_3OD (3:1) at 25 °C gave a major product with ^1H and ^{13}C resonances that correspond well with one of the isomers observed in neat CD_2Cl_2 and is assigned as **6a** on the basis of the IR spectrum. On warming to 60 °C (10 min), weak signals due to the *trans* isomer grew in, suggesting that isomerization **6a** → **6b** can occur.[27] Also observed after warming to 60 °C were $^{13}CH_3{}^{13}CO_2CD_3$ and the iridium hydride $[Ir(CO)_2I_3D/H]^-$ resulting from methanolysis of iridium acetyl species according to eq 3.

$$[Ir(^{13}CO)_2I_3(^{13}CO^{13}CH_3)]^- + CD_3OD/H \rightarrow [Ir(^{13}CO)_2I_3D/H]^- + {}^{13}CH_3{}^{13}CO_2CD_3 \quad (3)$$

When $[Ir(^{13}CO)_2I_3(^{13}CH_3)]^-$ was carbonylated with unlabeled CO in 25% MeOH/PhCl, $^1J_{C-C}$ doublets in the ^{13}C NMR spectra of **6a** and **6b** indicated doubly labeled $^{13}CO^{13}CH_3$ groups, showing that the methyl group migrates to a CO ligand already coordinated to Ir in **2**.

Careful choice of reaction conditions (see Experimental Section) enabled the isolation of **6** as an analytically pure solid, which ^1H NMR showed to contain **6a** and **6b** in a ca. 9:1 ratio. A crystal from this sample was selected for X-ray diffraction, the structure obtained being that of **6a** (Figure 5). The complex has distorted octahedral geometry with the acetyl ligand leaning away from the two *cis* iodide ligands to give a bond angle with the *trans* iodide of 173°. The plane of the acetyl ligand is twisted ca. 30° relative to the approximate mirror plane of the $Ir(CO)_2I_3$ fragment. The Ir−I bond *trans* to acetyl is longer by ca. 0.1 Å than those *trans* to CO due to the strong *trans* influence of acetyl.

Kinetics of Carbonylation of 2. In situ HPIR spectroscopy was used to follow the exponential decay of the 2093 cm^{-1} band of **2**. Observed first-order rate constants are reported in the Supporting Information (Tables S4−S6). In PhCl solvent the reaction rate was found to be independent of CO pressure above a threshold of ca. 3.5 barg. Variable-temperature kinetic data were measured over the range 80−122 °C, and an Eyring plot of these data gave the activation parameters listed in Table 1. Addition of Bu_4NI (equimolar with Ir) lowered the observed

(25) Isomers **6a** and **6b** were also identified in the NMR spectra of products recovered after carbonylation of **2** in PhCl (80 psig, 100 °C). ^1H NMR ($CDCl_3$): δ 2.77, 3.04 ($COCH_3$). ^{13}C NMR ($CDCl_3$): δ 49.6, 50.5 ($COCH_3$), δ 196.9, 197.8 ($COCH_3$), and δ 151.5, 160.5 (Ir-*C*O).

(26) Similarly, *fac*,*cis*-$[Rh(CO)_2I_3(COMe)]^-$ has ν(CO) at 2114 (s) and 2081 (s) cm^{-1}, while *mer*,*trans*-$[Rh(CO)_2I_3(COMe)]^-$ has ν(CO) at 2141 (vw) and 2084 (s) cm^{-1}. The low-frequency ν(CO) bands of *cis* and *trans* $[M(CO)_2I_4]^-$ (M = Rh, Ir) are also nearly coincident (Haynes, A.; McNish, J.; Pearson, J. M. *J. Organomet. Chem.* **1997**, *551*, 339).

(27) Another (unidentified) minor acetyl species showed δ ^1H 2.70 (dd, $^1J_{H-C}$ 128.4 Hz, $^2J_{H-C}$ 5.4 Hz), δ ^{13}C 203.9 (d, $^1J_{C-C}$ 32 Hz, *C*OCH_3, $COCH_3$ signal presumed hidden by solvent peaks) and 162.9 (Ir-*C*O).

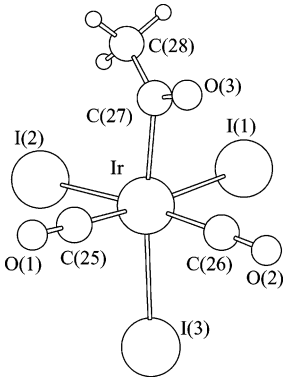

Figure 5. X-ray crystal structure of **6a**. Ph_4As^+ counterion omitted. Selected bond lengths (Å): Ir−C(25) 1.890(6), Ir−C(26) 1.903(5), Ir−C(27) 2.193(5), Ir−I(1) 2.6939(7), Ir−I(2) 2.7115(7), Ir−I(3) 2.8281(7), O(1)−C(25) 1.118(7), O(2)−C(26) 1.121(6), O(3)−C(27) 1.208(6), C(27)−C(28) 1.375(8). Selected bond angles (deg): C(25)−Ir−C(26) 96.5(2), C(25)−Ir−C(27) 91.4(2), C(26)−Ir−C(27) 90.2(2), C(27)−Ir−I(1) 85.20(12), C(27)−Ir−I(2) 95.34(12), I(1)−Ir−I(2) 92.688(13), C(27)−Ir−I(3) 172.93(12), O(1)−C(25)−Ir 178.5(6), O(2)−C(26)−Ir 177.7(5), O(3)−C(27)−C(28) 127.8(5), O(3)−C(27)−Ir 111.5(4), C(28)−C(27)−Ir 120.7(4).

rate constant by a factor of ca. 2, similar to the effect of iodide salts in the *catalytic* reactions.[28]

In a preliminary communication we reported that carbonylation of **2** to **6** is dramatically accelerated by the presence of methanol.[20] For example, addition of 1% MeOH (v/v) results in a ca. 10^4-fold rate enhancement at 33 °C (based on the extrapolated rate constant in PhCl using activation parameters measured at higher temperatures). Higher methanol concentrations gave an approximately linear increase in rate. Figure 6 shows the dependence of rate on CO pressure and added Ph_4AsI in 3:1 PhCl−MeOH. In the absence of iodide salt a saturation dependence on *p*CO is found. Substantial inhibition is caused by Ph_4AsI (2 molar equiv/Ir), but this decreases as the CO pressure is raised. The behavior of the model reaction closely resembles the kinetics of the catalytic carbonylation system (Table S2 and Figure 2).

Variable-temperature kinetic measurements in PhCl−MeOH gave quite different activation parameters (Table 1) from those in neat PhCl, with a much lower $\Delta H^{\ddagger}$ partly offset by a large negative $\Delta S^{\ddagger}$. Higher alcohols gave smaller rate enhancements, and a plot of ln k_{obs} vs the alcohol's Taft α value[29] shows a good linear correlation, indicating that the alcohol's hydrogen bond donor ability controls the rate. By contrast, addition of a polar aprotic donor solvent such as MeCN had only a small effect.

Mechanism of the Unpromoted Carbonylation of 2. Scheme 2 illustrates a mechanism for carbonylation of **2** consistent with the kinetic data presented above. Dissociative substitution of iodide by CO gives **4**, for which spectroscopic data indicate a *fac* tricarbonyl structure (vide infra). Theoretical calculations indicate that migratory insertion in **4** leads directly to **5a**, which has a square pyramidal geometry with an apical acetyl ligand (consistent with acetyl's large *trans* influence). Coordination of iodide to **5a** would give **6a**, whereas prior isomerization to **5b** would lead to **6b**. The selective formation

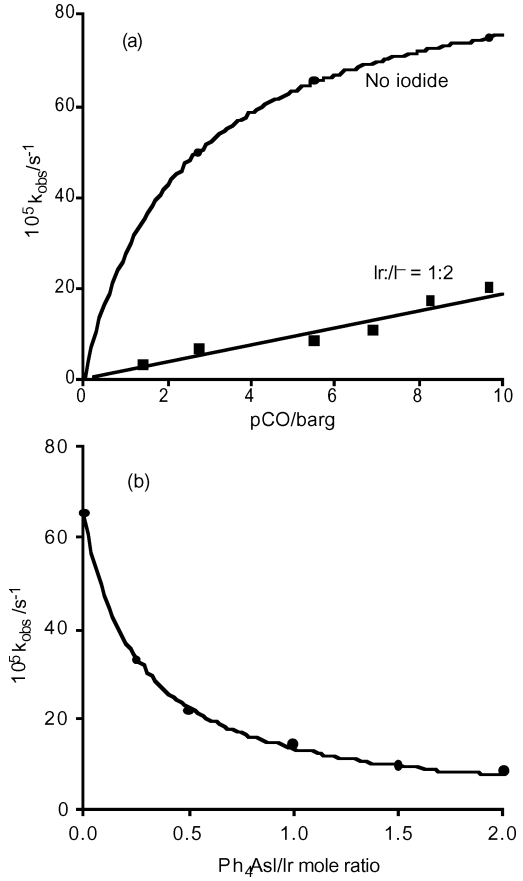

Figure 6. Plots of k_{obs} for carbonylation of **2** in PhCl−MeOH (3:1 v/v) at 33 °C: (a) effect of CO pressure in the absence or presence of Ph_4AsI (2 molar equiv per Ir); (b) effect of [Ph_4AsI] at 5.5 barg CO.

of **6a** as the kinetic product in PhCl−MeOH can be explained if **5a** is trapped by coordination of a methanol solvent molecule, preventing isomerization to **5b**. The mixture of isomers observed at high temperature may be under thermodynamic control, with isomerization occurring via loss of iodide or CO or via a tricarbonyl **7**.[30−32]

The accelerating effect of protic solvents such as methanol can be understood in terms of their ability to solvate an iodide anion. The large negative $\Delta S^{\ddagger}$ found at high [MeOH] likely results from strong solvation of the dissociating iodide ligand due to H-bonding interactions (eq 4). Alcohols also promote the reaction of **2** with phosphites to give acetyl complexes, $[Ir(CO)L_2I_2(COMe)]$ (L = $(P(OR)_3$),[33] and protic solvents facilitate other reactions that involve halide dissociation from a metal complex.[34]

$$[Ir(CO)_2I_3Me]^- \textbf{(2)} + n\ MeOH \rightleftharpoons [Ir(CO)_2I_2Me]\ \textbf{(3)} + (MeOH)_n\cdots I^- \quad (4)$$

Other migratory insertion reactions are promoted by good donor solvents[35] which coordinate to the vacant site created by

(28) Due to the low solubility of Ph_4AsI in PhCl, the effect of iodide salt was studied using Bu_4NI and the Bu_4N^+ salt of **2**. In the absence of added iodide salt Bu_4N^+[**2**] was carbonylated marginally slower than Ph_4As^+[**2**].
(29) Kamlet, M. J.; Abboud, J. L. M.; Taft, R. W. *Prog. Phys. Org. Chem.* **1981**, *13*, 485.
(30) In the Rh system, oxidative addition of acetyl iodide to $[Rh(CO)_2I_2]^-$ gives *fac*,*cis*-$[Rh(CO)_2I_3(COMe)]^-$, which isomerizes to the *mer*, *trans* geometry at room temperature (ref 32). The *mer*, *trans* isomer is formed directly from reaction of $[Rh(CO)I_3(COMe)]_2^{2-}$ with CO (ref 31).
(31) Adams, H.; Bailey, N. A.; Mann, B. E.; Manuel, C. P.; Spencer, C. M.; Kent, A. G. *J. Chem. Soc., Dalton Trans.* **1988**, 489.
(32) Howe, L.; Bunel, E. E. *Polyhedron* **1995**, *14*, 167.
(33) Haynes, A.; Pearson, J. M.; Vickers, P. W.; Charmant, J. P. H.; Maitlis, P. M. *Inorg. Chim. Acta* **1998**, *270*, 382.

alkyl migration, but in the case of **2** the ability to solvate an iodide anion appears more important. Strong coordination by solvent (e.g., MeCN) to Ir will also inhibit formation of the tricarbonyl **4** (vide infra).

Effect of Promoters on the Carbonylation of 2. In light of the beneficial effects of various metal compounds on catalytic carbonylation (vide supra), we tested the effects of some of these compounds on the kinetics of carbonylation of **2**. The effects of ruthenium and indium complexes were studied in detail to compare the two categories of promoter. As in the absence of promoters, acetyl products **6a** and **6b** were formed in a ca. 1:1 ratio in PhCl. Kinetic data are reported in the Supporting Information (Tables S5 and S6). Addition of the *neutral* ruthenium(II) iodocarbonyl complexes, $[Ru(CO)_3I_2]_2$, $[Ru(CO)_4I_2]$, or $[Ru(CO)_2I_2]_n$ (Ru/Ir molar ratio <0.2), was found to give substantial rate enhancements (by factors of 15−20 for a Ru:Ir ratio of 1:13 at 93 °C, PhCl). Indium and gallium triiodides and zinc diiodide gave accelerations very similar to the neutral ruthenium species.[36,37] By contrast, addition of *anionic* ruthenium(II) species $[Ru(CO)_3I_3]^-$ or $[Ru(CO)_2I_4]^{2-}$ (as their Bu_4N^+ salts) did not lead to any appreciable promotion *or* inhibition. This behavior reflects that found in the catalytic system where the promotional effect of $[Ru(CO)_4I_2]$ was negated by the presence of an equimolar quantity of LiI (equivalent to addition of $Li[Ru(CO)_3I_3]$). The effectiveness of neutral, but not anionic Ru complexes indicates that the ability to accept an iodide ligand is a key property of the promoter.

The effect of promoter concentration on the rate of carbonylation of **2** is illustrated graphically in Figure 7. The effect is proportional to [promoter] at low concentrations, but some leveling-off is evident at higher [promoter]/[Ir] ratios, particularly for $[Ru(CO)_3I_2]_2$. The graph shows that the promoters all give similar rate enhancements at a given temperature and [promoter]/[Ir] ratio. Increasing CO pressure was found to have little effect on the reaction rate in the presence of promoter. The activation parameters (Table 1) derived from Eyring plots show a substantial lowering of $\Delta H^{\ddagger}$ and a change from positive to negative $\Delta S^{\ddagger}$ on addition of promoter. In mixed PhCl−MeOH solvent systems (25−50% MeOH, v/v) significant promotion was evident only on addition of larger quantities of $[Ru(CO)_3I_2]_2$ (e.g., Ru:Ir = 2:5).

Stoichiometric Iodide Transfer Reactions. Complex **2** was found to react cleanly with a small excess of GaI_3 or InI_3 in CH_2Cl_2, to give a product with ν(CO) bands (2118 and 2074 cm^{-1}) consistent with formation of a neutral species. The reaction of **2** with zinc diiodide also gave some of the same product, but did not go to completion, perhaps due to solubility limitations. From the reaction of **2** with InI_3 on a preparative scale, a dimeric neutral iridium methyl complex, $[Ir(CO)_2I_2Me]_2$ (**3d**), was isolated and characterized spectroscopically and by X-ray crystallography.[38,39]

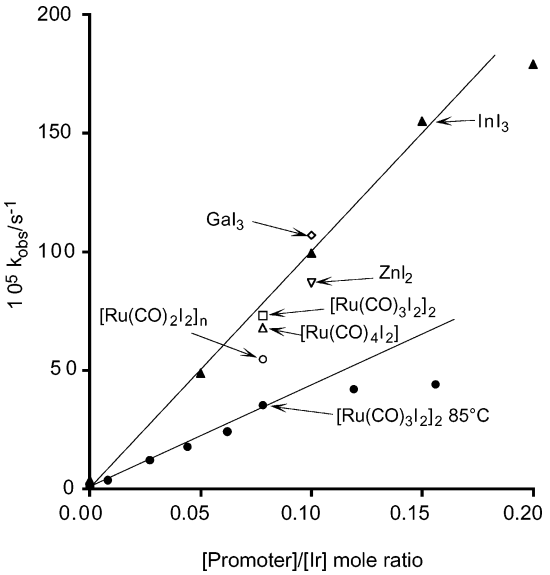

Figure 7. Plots of k_{obs} for carbonylation of **2** vs [promoter] in PhCl (at 5.5 barg and 93 °C unless stated otherwise).

NMR spectroscopy showed the presence of two isomers of **3d** in CD_2Cl_2 solution in the approximate ratio 5:2, consistent with the data reported by Gautron et al.[39] Molecular weights determined for solutions of **3d** by osmometry were 1001 in PhCl (consistent with the dimeric structure; MW 1034) and 538 in MeCN, indicating bridge cleavage by the coordinating solvent. This was confirmed by the observation of ν(CN) at 2338 cm^{-1} for $[Ir(CO)_2(NCMe)I_2Me]$ in 3% v/v MeCN−$CHCl_3$, along with a shift of ν(CO) to 2126 and 2080 cm^{-1}. Addition of 2 equiv of I^- to the dimer quickly regenerates the anion, **2**. Similarly, InI_3 was found to abstract iodide from the acetyl complex **6a** to give $[Ir(CO)_2I_2(COMe)]_2$[14] (ν(CO) (CH_2Cl_2) 2124, 2081, and 1712 cm^{-1}), and addition of Bu_4NI resulted in rapid conversion back to **6a**.

The reaction of **2** with $[Ru(CO)_3I_2]_2$ resulted in quite complicated IR spectra. On mixing CH_2Cl_2 solutions of $[Ru(CO)_3I_2]_2$ and **2** (to attain eqimolar [Ir] and [Ru]), the ν(CO) bands due to both starting complexes decayed slowly, to be replaced by new absorptions at 2119 sh, 2103 s 2074 w, 2060 sh, 2048, and 2038 m. The spectrum is consistent with the presence of some $[Ru(CO)_3I_3]^-$ and **3d**, but the additional absorptions are not due to known Ir or Ru complexes. The reaction of **3d** and $Bu_4N[Ru(CO)_3I_3]$ in CH_2Cl_2 resulted in a similar IR spectrum after several minutes. The new product is tentatively assigned as a mono-iodide-bridged Ir−Ru dimer **15** (Scheme 4), which would be expected to exhibit up to five ν(CO) bands. ^{13}C NMR measurements on this system support the formation of a mixed dimer of this sort.[40] Evidence for a

(34) Bennett, M. A.; Crisp, G. T. *Organometallics* **1986**, *5*, 1792. Bennett, M. A.; Crisp, G. T. *Organometallics* **1986**, *5*, 1800. Romeo, R.; Minniti, D.; Lanza, S. *Inorg. Chem.* **1980**, *19*, 3663. Kelm, H.; Louw, W. J.; Palmer, D. A. *Inorg. Chem.* **1980**, *19*, 843. Treichel, P. M.; Vincenti, P. J. *Inorg. Chem.* **1985**, *24*, 228. Blum, O.; Milstein, D. *J. Am. Chem. Soc.* **1995**, *117*, 4582.

(35) Mawby, R. J.; Basolo, F.; Pearson, R. G. *J. Am. Chem. Soc.* **1964**, *86*, 3994. Butler, I. S.; Basolo, F.; Pearson, R. G. *Inorg. Chem.* **1967**, *6*, 2074.

(36) Despite the promotional effect of $[W(CO)_6]$ on the catalytic process, neither $[W(CO)_6]$ nor $[Cr(CO)_6]$ had any effect on the rate of carbonylation of **2**. Although group 6 metal hexacarbonyls are known to react with iodide salts on heating to give $[M(CO)_5I]^-$ (ref 37), it appears that iodide abstraction by these reagents is not efficient under the conditions of our experiments. Aluminum triiodide was also tested, but found not to be effective.

(37) Abel, E. W.; Butler, I. S.; Reid, J. G. *J. Chem. Soc.* **1963**, 2068. Palitzsch, W.; Beyer, C.; Böhme, U.; Rittmeister, B.; Roewer, G. *Eur. J. Inorg. Chem.* **1999**, 1813.

(38) Since our preliminary communication (ref 21), an X-ray structure of **3d** has also been reported independently (ref 39). The two structures show no significant differences. Crystallographic data for our structure are listed in the Supporting Information.

(39) Gautron, S.; Giordano, R.; Le Berre, C.; Jaud, J.; Daran, J.-C.; Serp, P.; Kalck, P. *Inorg. Chem.* **2003**, *42*, 5523.

(40) ^{13}C NMR data have recently been reported for **15**, formed by reaction of $[Ru(CO)_4I_2]$ with **2**. Under 6 bar CO **15** is cleaved to give **4** and $[Ru(CO)_3I_3]^-$, demonstrating iodide transfer from Ir to Ru. Whyman, R.; Wright, A. P.; Iggo, J. A.; Heaton, B. T. *J. Chem. Soc., Dalton Trans.* **2002**, 771.

Table 2. Reaction Energies (kJ mol^{-1}) Calculated at the MP2 Level (2DZ and 2DZ* bases) for Selected Ligand Substitution, Transfer, and Interchange Processes[a]

reactant(s)	products	ΔE/kJ mol^{-1} vacuum 2DZ	vacuum 2DZ*	PhCl 2DZ	MeOH 2DZ
	CO/Iodide Substitution				
2 + CO	**4** + I^-	87.1	115.9	−11.4	−27.8
	Iodide Transfer				
2 + $[Ru(CO)_3I_2]$	**3** + $[Ru(CO)_3I_3]^-$	−55.8	−48.4	−56.9	−59.4
6a + $[Ru(CO)_3I_2]$	**5a** + $[Ru(CO)_3I_3]^-$	−82.3	−85.4[b]	−83.2	−83.1
1 + $[Ru(CO)_3I_2]$	**8** + $[Ru(CO)_3I_3]^-$	11.7	−1.7	6.7	8.6
2 + InI_3	**3** + InI_4^-	−44.5	−35.1	−38.8	−42.8
6a + InI_3	**5a** + InI_4^-	−71.0	−70.5[b]	−65.1	−66.5
1 + InI_3	**8** + InI_4^-	23.0	11.6	24.8	25.2
	Iodide/CO Interchange				
2 + $[Ru(CO)_4I_2]$	**4** + $[Ru(CO)_3I_3]^-$	5.3	0.8	8.0	9.9
6a + $[Ru(CO)_4I_2]$	**7** + $[Ru(CO)_3I_3]^-$	10.7	8.8[b]	3.6	2.1
1 + $[Ru(CO)_4I_2]$	**9** + $[Ru(CO)_3I_3]^-$	10.8	−0.1	11.7	17.8
	Iodide/Solvent Interchange				
2 + $[Ru(OH_2)(CO)_3I_2]$	$[Ir(OH_2)(CO)_2I_2Me]$ + $[Ru(CO)_3I_3]^-$	−7.5	−8.0[b]		
1 + $[Ru(OH_2)(CO)_3I_2]$	$[Ir(OH_2)(CO)_2I]$ + $[Ru(CO)_3I_3]^-$	2.1	5.2		

[a] Solvent effects (in PhCl, $\epsilon = 5.7$; MeOH, $\epsilon = 33$) were calculated using the PCM method. [b] Single-point 2DZ* calculations on 2DZ optimized structures.

Scheme 3. Reversible Iodide Abstraction from **2** Leading to **3d**

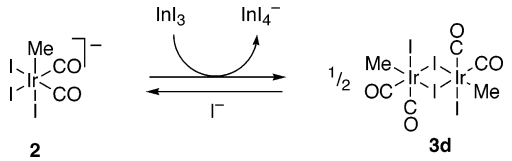

Scheme 4. Anionic Iodide-Bridged Dimers **15** and **16**

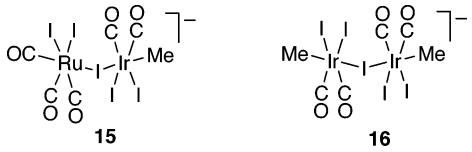

similar Ir-only species was also found in the reaction between **2** and **3d** in CH_2Cl_2 or by adding substoichiometric amounts of Bu_4NI to **3d**.[41] In each case a product assigned as **16** is observed (ν(CO) 2108, 2060 cm^{-1}; δ ^{1}H 2.3 in $CDCl_3$), which exists only in an equilibrium with **2** and **3d** and cannot be isolated. Dimers **15** and **16** are not observed in polar solvents such as MeCN or $MeNO_2$ and are probably not significant catalytic intermediates.

Ab Initio Calculations for Iodide Transfer. Reaction energies for dissociation of iodide, CO, and solvent (H_2O or MeOH) were computed by ab initio (MP2) theoretical methods for the important Ir, Ru,[42−44] and In species (Supporting Information, Table S11). Solvent medium effects were considered by the PCM method using the dielectric constants of PhCl ($\epsilon = 5.7$) and MeOH ($\epsilon = 33$).[45] Selected reaction energies derived from combination of the appropriate ligand dissociation energies are listed in Table 2.

Substitution of an iodide ligand in **2** by CO to give **4** is predicted to be highly endothermic in vacuo, but exothermic by 11 or 28 kJ mol^{-1} in PhCl or MeOH, respectively. Cheong et al. calculated the same substitution reaction to be endothermic by 17 kJ mol^{-1} in PhCl.[46] Solvent effects are less pronounced for reactions where an iodide ligand is transferred between metal centers, as the solvation energies of reactants and products are similar. Iodide transfer from **2** to $[Ru(CO)_3I_2]$ or InI_3 is predicted to be exothermic (by ca. 50 and 40 kJ mol^{-1}, respectively). The corresponding reactions of **6a** are even more exothermic, whereas iodide transfer from **1** to $[Ru(CO)_3I_2]$ or InI_3 is slightly endothermic, indicating that Ir(I) binds iodide more effectively than Ir(III). For ligand *interchange* processes in which a CO or solvent ligand from Ru is exchanged with an iodide from Ir, the reaction energies are much smaller (0 ± ca.10 kJ mol^{-1}) than those for iodide *transfer*. Thus interchange of iodide and solvent (or CO) ligands between iridium and ruthenium centers is thermodynamically feasible.

Reactivity of *fac,cis*-$[Ir(CO)_3I_2Me]$ (4). The spectroscopic characterization and reactivity of the neutral tricarbonyl **4** has been reported in a preliminary communication.[21] The complex is generated by reaction of the dimer **3d** with CO in CH_2Cl_2 or PhCl. IR, ^{13}C NMR, and ^{1}H NMR spectroscopic data for **4** are given in the Supporting Information (Table S8 and Figure S6). Three ν(CO) bands of similar intensity are consistent with a *fac*-tricarbonyl geometry for **4**. Using 1 atm CO, less than 10% conversion of **3d** into **4** was achieved, but essentially complete conversion occurs under 27.5 barg CO. On venting the CO and introduction of an inert atmosphere, **4** reverts to **3d** over several minutes. When acetonitrile was used as solvent, formation of **4** was suppressed even at high CO pressures, presumably due to cleavage of the dimer and occupation of the vacant site by MeCN.

Isotopic labeling experiments indicated that when unlabeled **3d** reacts with ^{13}CO, the incoming ^{13}CO ligand coordinates *trans* to the methyl group. When the ^{13}CO atmosphere was removed, $[Ir(CO)_2(^{13}CO)I_2Me]$ was found to revert cleanly to $[Ir(CO)_2I_2Me]_2$, with no detectable retention of isotopic label. The reversible reaction of **3d** with ^{13}CO is therefore stereospecific,

(41) The ν(CO) bands of **16** were also observed during reactions between **2** and InI_3 or GaI_3 in CH_2Cl_2.
(42) The preferred geometrical isomers of ruthenium iodocarbonyl complexes (*cis*-$[Ru(CO)_4I_2]$ (ref 43) and *fac*-$[Ru(CO)_3I_3]^-$ (ref 44)) were correctly predicted by single-point 2DZ* calculations on the 2DZ optimized geometries (Table S9). The five-coordinate $[Ru(CO)_3I_2]$ was taken to have a *fac*-$Ru(CO)_3$ unit.
(43) Dahl, L. F.; Wampler, D. L. *Acta Crystallogr.* **1962**, *15*, 946.
(44) Zoeller, J. R. *Inorg. Chem.* **1986**, *25*, 3933. Galletti, A.; Braca, G.; Sbrana, G.; Marchetti, F. *J. Mol. Catal.* **1985**, *32*, 291.
(45) Despite their different characters, the dielectric constants of acetic acid ($\epsilon = 6.2$) and chlorobenzene ($\epsilon = 5.7$) are remarkably similar. The actual dielectric constant of the catalytic reaction solvent will be modified by temperature and the presence of other species, particularly water.
(46) Cheong, M.; Schmid, R.; Ziegler, T. *Organometallics* **2000**, *19*, 1973.

Scheme 5. Stereochemistry of Reaction of ^{13}CO with **3d**[a]

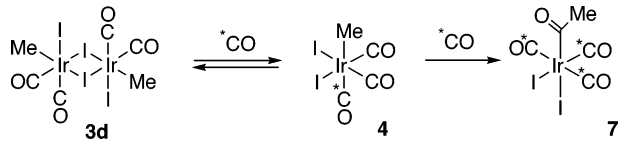

[a] The extent of labeling in the terminal carbonyls of **7** is undetermined.

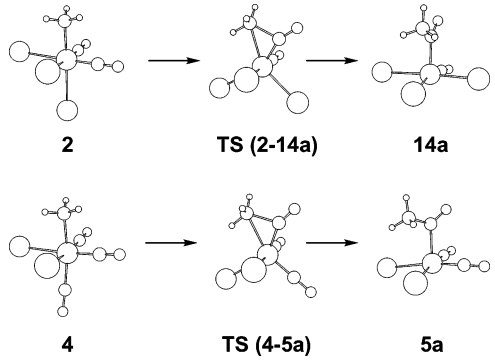

Figure 8. Optimized structures (MP2/LANL2DZ) for stationary points on the reaction coordinate for migratory CO insertion in complexes **2** and **4**.

with the labeled ligand entering and leaving from the site *trans* to methyl, as shown in Scheme 5.

When a solution of **4** under CO pressure was warmed above 40 °C, the ν(CO) bands of **4** were replaced by new absorptions due to $[Ir(CO)_3I_2(COMe)]$ (**7**), which is assigned a *mer*-tricarbonyl geometry. This is confirmed by the ^{13}C NMR spectrum of $[Ir(^{13}CO)_3I_2(^{13}COMe)]$, which displayed no $^2J_{C-C}$ coupling for the acetyl carbonyl, consistent with all three ^{13}CO ligands being *cis* to acetyl. The spectrum of **7** generated from the reaction of unlabeled **3d** with ^{13}CO indicated no incorporation of ^{13}CO into the acetyl group, consistent with the mechanism shown in Scheme 5. On releasing the CO pressure, **7** was observed to convert slowly into $[Ir(CO)_2I_2(COMe)]_2$ (ν(CO) 2123, 2091, 1708 cm^{-1}), resulting from loss of CO.[14]

Pseudo-first-order rate constants for the migratory insertion reaction of **4** in PhCl (27.5 barg CO, 44−85 °C) are listed in the Supporting Information (Table S7), and an Eyring plot of these data yields the activation parameters given in Table 1. Complex **4** is carbonylated more than 700 times faster than the anion **2** at 85 °C, representing a lowering of $\Delta G^{\ddagger}$ by 20 kJ mol^{-1}. Extrapolation to higher temperatures using the measured activation parameters reduces the difference in rates, but even at 180 °C, **4** is predicted to react an order of magnitude faster than **2**. Substitution of iodide by CO is also known to facilitate methyl migration in $[Fe(CO)_2(PMe_3)_2IMe]$.[47] Addition of small amounts of methanol was found to accelerate the carbonylation of **4** (see Table S7) but not to the dramatic extent found for **2**. Activation parameters calculated for the reaction in 1% MeOH−PhCl show a modest decrease in $\Delta H^{\ddagger}$ and more negative $\Delta S^{\ddagger}$ than in the absence of methanol (Table 1).

Ab initio calculations (at the MP2 level) have been performed on migratory insertion in **2** and **4**, and stationary points on the reaction coordinates are depicted in Figure 8. In both transition states, formation of the acetyl C−C bond is accompanied by opening of the bond angle between ligands *trans* to the methyl and CO ligands. After passing through the transition state this angle continues to open, to give a square pyramidal product (**14a** or **5a**) with an apical acetyl ligand. This is attributable to the strong *trans* influence of acetyl and provides an explanation why the kinetic products of migratory CO insertion often have the entering ligand *trans* to acetyl,[48] rather than *cis* as found in the classic $[Mn(CO)_5Me]$ system.[49]

Table 3. Calculated Activation Energies ($\Delta E^{\ddagger}$) and Reaction Energies (ΔE_{mig}) for Migratory CO Insertion in **2** and **4** and Calculated Reaction Energies (ΔE_{CO}) for Carbonylation of **2** and **4** to Give **6a** and **7**, Respectively (values in kJ mol^{-1})

reactant	method	$\Delta E^{\ddagger}$	ΔE_{mig}	ΔE_{CO}
$[Ir(CO)_2I_3Me]^-$, **2**	MP2 2DZ*	149.0	46.2	−64.7[a]
	ADF[46]	124.7	14.8	
	B3LYP[50]	117.6	−10.9	
$[Ir(CO)_3I_2Me]$, **4**	MP2 2DZ*	102.1	16.4	−58.8[a]
	ADF[46]	78.2	−12.2	
	B3LYP[50]	82.8	−29.3	

[a] Single-point 2DZ* calculation on 2DZ optimized structures.

While this work was in progress, two DFT studies of the same reactions were reported,[46,50] and the computed activation and reaction energies are summarized along with ours in Table 3. All the theoretical methods predict that methyl migration in **4** has a substantially lower activation barrier (by between 35 and 47 kJ mol^{-1}) and is more exothermic than the corresponding reaction of **2**. Our ab initio (MP2) activation energy slightly overestimates the experimental $\Delta H^{\ddagger}$ for carbonylation of **4** (89 (±3) kJ mol^{-1}), whereas the DFT calculations underestimate the barrier by a similar amount.[51] Consideration of solvent effects (using the PCM method) has only a marginal effect on the activation barriers.

The lower activation barrier for migratory CO insertion in **4** has been attributed previously to the ability of a *trans* CO ligand to labilize the Ir−Me bond, combined with stabilization of the transition state by an additional π-acceptor CO ligand.[46,50] The computational data show the Ir−Me bond to be only marginally longer (by 0.01 Å) in **4** than in **2**, and estimated Ir−Me bond dissociation energies actually indicate a *stronger* Ir−Me bond in **4**.[52] A larger perturbation is found for the Ir−CO bond distances *cis* to methyl in **2** (1.87 Å) and **4** (1.92 Å), reflecting a decrease in π-back-donation from the Ir center in **4**. This is also apparent in the average ν(CO) values, which shift to high frequency by 27% (experimental) and 23% (theoretical) for **4** compared with **2**. Weaker back-donation from Ir in **4** depopulates the CO π^* orbitals,[53] thereby raising the electrophilicity of the carbonyl ligand and promoting methyl migration (which can be regarded as an intramolecular nucleophilic attack).

(47) Cardaci, G.; Reichenbach, G.; Bellachioma, B.; Wassink, B.; Baird, M. C. *Organometallics* **1988**, *7*, 2475. Bellachioma, B.; Cardaci, G.; Macchioni, A.; Reichenbach, G.; Foresti, E.; Sabatino, P. *J. Organomet. Chem.* **1997**, *531*, 227. Wright, S. C.; Baird, M. C. *J. Am. Chem. Soc.* **1985**, *107*, 6899.

(48) Alonso, F. J. G.; Llamazares, A.; Riera, V.; Vivanco, M.; Granda, S.; Diaz, M. R. *Organometallics* **1992**, *11*, 2826. Glyde, R. W.; Mawby, R. J. *Inorg. Chim. Acta* **1971**, *5*, 317. Barnard, C. F. J.; Daniels, J. A.; Mawby, R. J. *J. Chem. Soc., Dalton Trans.* **1979**, 1331.

(49) Noack, K.; Calderazzo, F. *J. Organomet. Chem.* **1967**, *10*, 101. Flood, T. C.; Jensen, J. E.; Statler, J. A. *J. Am. Chem. Soc.* **1981**, *103*, 4410.

(50) Kinnunen, T.; Laasonen, K. *J. Mol. Struct. (THEOCHEM)* **2001**, *542*, 273.

(51) The ab initio activation barrier for migratory insertion in **2** is very similar to the experimental $\Delta H^{\ddagger}$ for carbonylation of **2** in PhCl, but the validity of a direct comparison is doubtful due to the competing neutral pathway in the experimental studies.

(52) The Ir−Me bond energy is estimated to be 40 kJ mol^{-1} stronger for **4** than for **2** on the basis of calculated energies (before relaxation) of the homolysis products CH_3 and $[Ir(CO)_xI_y]^{n-}$ ($x = 2$ or 3, $y = 3$ or 2, $n = 1$ or 0).

(53) In support of this, Mulliken population analysis indicates that the partial charge on the carbon of a CO *cis* to methyl decreases from +0.32 in **4** to +0.26 in **2**. Also the appropriate unoccupied acceptor orbital (an out of phase combination of π^*CO with dπ) is significantly higher in energy for **2** than for **4** (0.160 and 0.039 hartrees respectively).

Scheme 6. Mechanism for Promotion of Carbonylation of **2** by Iodide Abstractors

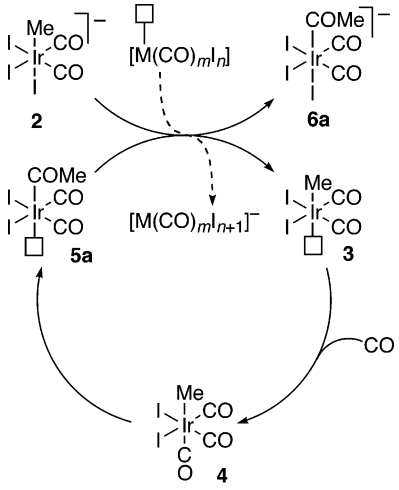

Mechanism for Promotion of Carbonylation of 2. It has been demonstrated that (i) iodide transfer from **2** to promoter species is facile and (ii) the neutral species **4** is carbonylated much more readily than **2**. We can therefore propose a mechanism in which an iodide ligand is initially transferred from **2** to the promoter, allowing coordination of CO to Ir to give **4**. Migratory insertion then proceeds to form **5a**. Iodide transfer from the promoter back to Ir at this point is unlikely, given that InI_3 abstracts iodide from **6a** (vide supra). Instead, an iodide ligand could be transferred between iridium centers as shown in Scheme 6. In this scenario the additive (e.g., InI_3, or $[Ru(CO)_3I_2]_2$) behaves more like an initiator, abstracting iodide to generate **3**, as shown by the dashed arrow in Scheme 6. The anion InI_4^- or $[Ru(CO)_3I_3]^-$ then acts as a spectator, with promotion being propagated by an iodide "hole" introduced by the iodide abstractor. Such a mechanism can operate if the Ir(III) methyl and acetyl complexes have similar affinities for iodide, such that the equilibrium **2** + **5a** ⇌ **3** + **6a** does not lie heavily to the left.[54]

We tested this hypothesis by investigating the kinetics of carbonylation of **2** in the presence of substoichiometric amounts of **3d**. This regime mimics the iodide abstracting effect of a promoter such as $[Ru(CO)_3I_2]$ or InI_3, by introducing a proportion of the neutral iridium complex, but avoids any direct promoter−Ir interactions. The data obtained (Table S6) show that addition of **3d** causes a rate enhancement very similar to that of other metal promoters. Variable-temperature data gave activation parameters comparable to those obtained for $[Ru(CO)_3I_2]_2$ and InI_3 additives (Table 1). Thus the key role of the promoter is to perturb the ratio of anionic and neutral iridium complexes, and the effect can be mimicked by deliberate tuning of this ratio in an Ir-only system.

These results argue against the participation of a more direct interaction between the promoter and the iridium center such as redox processes or heterodi- or poly-nuclear complexes.[55] Classic studies by Shriver and co-workers[56] showed that certain Lewis acids (e.g., $AlCl_3$) can effect dramatic accelerations of migratory CO insertion (for example in $[Mn(CO)_5Me]$), by accepting a coordinate bond from the carbonyl oxygen of the incipient acyl ligand. An analogous intramolecular interaction has also been invoked to explain promotion of methyl migration in $[FeW(CO)_9Me]^-$ relative to $[Fe(CO)_4Me]^-$.[57] Although such interactions might play a minor role in the promotion of carbonylation of **2**, our results show clearly that the major role of the promoter is as an iodide acceptor.

Comparison of Kinetic Data for Model and Catalytic Reactions. Activation parameters for stoichiometric carbonylation of **2** and **4** and catalytic carbonylation of methanol are gathered in Table 1. The activation parameters for catalytic reactions in acetic acid are best matched by those for carbonylation of **2** in PhCl in the presence of a promoter ($[Ru(CO)_3I_2]_2$ or InI_3). Extrapolation of the appropriate Eyring plots gives a satisfactory prediction of catalytic rates. Although the reaction medium (and counterion) clearly differ,[45] it appears that the catalytic reaction is modeled reasonably well by the stoichiometric reaction of **2** with CO. Substantially different activation parameters were found for the model reaction in 3:1 PhCl−MeOH. The relatively small $\Delta H^{\ddagger}$ and large negative $\Delta S^{\ddagger}$ arise from associative assistance of iodide dissociation from **2** by methanol (eq 4). These parameters correspond very closely with those calculated from the catalytic data in 2:1 acetophenone−methanol reported by Matsumoto et al.[16,58] Thus the catalytic rate at high [MeOH] is also well modeled by our rate data for the carbonylation of **2**.

Promoters gave much larger rate enhancements for the model reactions than for the catalytic system. For example, a promoter: Ir ratio of 1:10 gave a 20−30-fold acceleration of the carbonylation of **2** in PhCl, whereas a 10-fold excess of promoter over Ir gave only a 2−3-fold improvement of catalytic activity (Figure 2). The difference in solvent is undoubtedly important, since PhCl will solvate iodide ions much less strongly than the catalytic medium. Consistent with this, larger concentrations of promoter were required to accelerate the carbonylation of **2** in a mixed PhCl−MeOH solvent system than in neat PhCl.

Activation parameters for the reaction of MeI with **1**[19] can be used to predict a second-order rate constant of ca. 11 $dm^3\ mol^{-1}\ s^{-1}$ at 190 °C, corresponding to a pseudo-first-order rate constant (at 0.4 M MeI) of 4.5 s^{-1}. To achieve the observed catalytic rate (in the absence of promoter) would require the

(54) This was demonstrated by ^1H NMR spectroscopy: an MeCN solution containing equimolar **6a** and **3**−NCMe attained an equilibrium in which ca. 50% of **3**−NCMe was converted into **2**.

(55) The mixed-metal cluster anions $[M_3Ir(CO)_{13}]^-$ (M = Ru, Os) have been used as catalyst precursors for methanol carbonylation, but under catalytic conditions they fragment to give $[Ir_4(CO)_{12}]$ and $[M(CO)_3I_3]^-$: Suss-Fink, G.; Haak, S.; Ferrand, V.; Stoeckli-Evans, H. *J. Mol. Catal. A-Chem.* **1999**, *143*, 163.

(56) Butts, S. B.; Strauss, S. H.; Holt, E. M.; Stimson, R. E.; Alcock, N. W.; Shriver, D. F. *J. Am. Chem. Soc.* **1980**, *102*, 5093. Richmond, T. G.; Basolo, F.; Shriver, D. F. *Inorg. Chem.* **1982**, *21*, 1272.

(57) Arndt, L. W.; Bancroft, B. T.; Darensbourg, M. Y.; Janzen, C. P.; Kim, C. M.; Reibenspies, J.; Varner, K. E.; Youngdahl, K. A. *Organometallics* **1988**, *7*, 1302.

(58) Matsumoto (ref 16) proposed rate-determining methanolysis of Ir(III)−COMe on the basis of rate dependence on [MeOH] and isolation of $[Ir(CO)(PPh_3)_2I_2(COMe)]$ on addition of PPh_3 to the cooled catalytic reaction mixture. However, ref 33 shows that P-donor ligands can induce CO insertion in **2** to give products of this type, so isolation of an Ir-acetyl does not show it to be the catalytic resting state. Methanolysis of **6** to give MeOAc is slow at ambient temperature but observable at ca. 50 °C. The much higher temperature and presence of water make it likely that solvolysis of **6** is relatively fast under process conditions. A pre-equilibrium **2** + CO = **6** followed by rate-determining solvolysis of **6** would result in a first-order dependence on [CO], which is not observed. Although **6** reverts to **2** + CO on heating in the absence of added CO, the equilibrium favors **6** even at 5 bar CO. Therefore if solvolysis of **6** were rate-determining, one would expect to observe it (rather than **2**) as the resting state at higher *p*CO.

Scheme 7. Mechanism for Promoted Iridium-Catalyzed Methanol Carbonylation

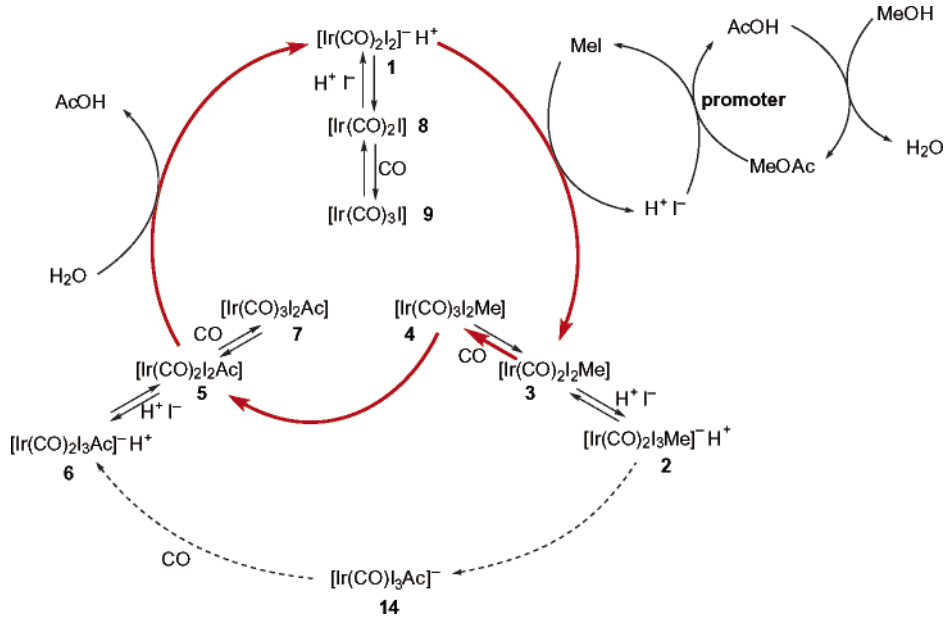

concentration of **1** to be ca. 0.5 mM or 5% of the total iridium concentration, consistent with the observation of weak IR bands due to **1** during catalysis. Similarly the rate constant for migratory insertion in **4** is estimated as 12 s^{-1} at 190 °C, requiring the concentration of **4** to be 0.2 mM (or 2% of the total Ir) to sustain the observed catalytic rate. The kinetics measured for the model reactions are therefore consistent with complexes **1** and **4** being intermediates in the catalytic cycle, but with most of the iridium existing in the form of the resting state **2**.

Catalytic Mechanism. A catalytic mechanism consistent with the data is shown in Scheme 7. The participating iridium complexes are grouped into three sets, namely, Ir(I) species, Ir(III)-methyls, and Ir(III)-acetyls. The three complexes within each set are linked by equilibria involving I^- and CO, and the dominant route for catalytic turnover is indicated by the red arrows. The interconversions of Ir species represented in Scheme 7 are essentially equivalent to Forster's mechanism (Scheme 1). However, we prefer to view the catalytic process as one rather than two cycles, with the process conditions influencing the nature of the catalyst resting state rather than the active cycle. We also depict the net oxidative addition of **1** + MeI → **2** as proceeding via **3**, resulting from initial S_N2 attack[50,59] by Ir(I).

Under the conditions of highest activity, the catalyst resting state is **2**, which sits outside the main catalytic loop. Added iodide salts will favor the equilibria leading to **2**, thus lowering the standing concentrations of **3** and **4** within the main loop and inhibiting the carbonylation rate. Similar inhibition is caused by raising the water concentration (above 5% w/w, Figure 1), which will lead to an increase in [I^-], according to eq 5. Similarly, the strong positive dependence of catalytic rate on [MeOAc][8,9] can be understood in terms of it reducing the steady state concentration of I^-.

$$\mathrm{MeOAc} + \mathrm{H_3O^+} + \mathrm{I^-} \rightleftharpoons \mathrm{MeI} + \mathrm{H_2O} + \mathrm{AcOH} \quad (5)$$

Methyl migration in **2** (indicated by the dashed arrows in Scheme 7) may make a minor (≤5%) contribution to catalytic turnover.[60] Assuming that the steady state concentration of **4** is less than 5% of the total [Ir] (since it is not observed by in situ IR), we can estimate that methyl migration must be at least 200 times faster for **4** than for **2** at 190 °C. This would require that $\Delta G^{\ddagger}$ is at least 20 kJ mol^{-1} lower for **4** than for **2**, consistent with experimental and computational results.

If the water concentration is decreased below 5% w/w, the catalytic rate diminishes and catalyst resting state shifts to the neutral Ir(I) tricarbonyl **9**. According to eq 5, low [H_2O] will afford a low [I^-], which is insufficient to sustain the iridium catalyst in a predominantly anionic form. Under these conditions, the equilibria[61] at the top of Scheme 7 are shifted toward **9**, which accumulates due to its low nucleophilicity toward MeI relative to **2**.[62]

Role of Promoters. The model stoichiometric reactions show that neutral compounds such as $[Ru(CO)_3I_2]_2$ and InI_3 are capable of abstracting iodide from complex **2** and promoting its carbonylation. In the catalytic process, the situation is somewhat more complex, as iridium complexes are not the sole source of iodide for the promoter to bind. HPIR spectroscopy showed that a ruthenium promoter exists as a mixture of $[RuCO)_2I_2(sol)_2]$, $[RuCO)_3I_2(sol)]$, and $[RuCO)_3I_3]^-$ in the absence of Ir, but that $[RuCO)_3I_3]^-$ becomes the dominant Ru species after injection of the Ir catalyst. Each turnover of the iridium cycle (Scheme 7) generates 1 molar equiv of HI

(59) Fulford, A.; Hickey, C. E.; Maitlis, P. M. *J. Organomet. Chem.* **1990**, *398*, 311. Ivanova, E. A.; Gisdakis, P.; Nasluzov, V. A.; Rubailo, A. I.; Rösch, N. *Organometallics* **2001**, *20*, 1161. Griffin, T. R.; Cook, D. B.; Haynes, A.; Pearson, J. M.; Monti, D.; Morris, G. E. *J. Am. Chem. Soc.* **1996**, *118*, 3029. Rendina, L. M.; Puddephatt, R. J. *Chem. Rev.* **1997**, *97*, 1735. Labinger, J. A.; Osborn, J. A. *Inorg. Chem.* **1980**, *19*, 3230.

(60) The estimated contribution of methyl migration in **2** to the catalytic activity is based on the rate measured at 15:1 LiI:Ir, which is ca. 10% of the rate in the absence of LiI. Since the in situ HPIR shows the Ir speciation to be >90% and ca. 50% **2**, respectively, with or without LiI, methyl migration in **2** can account for ≤5% of the catalytic rate in the absence of LiI.

(61) Quantitative studies of the equilibrium **1** + CO = **9** + I^- have recently been undertaken by Merbach and co-workers: Churland, R.; Frey, U.; Metz, F.; Merbach, A. E. *Inorg. Chem.* **2000**, *39*, 304; **2000**, *39*, 4137.

(62) The second-order rate constant for oxidative addition of MeI to neutral $[Ir(CO)_2(NCMe)I]$ (ν(CO)/cm^{-1}: 2078, 2006; generated by reaction of **1** with InI_3 in MeCN) is ca. 200 times smaller (1.56×10^{-5} dm^3 mol^{-1} s^{-1}) than that for **1** (3.09×10^{-3} dm^3 mol^{-1} s^{-1}) (25 °C, MeCN).

Scheme 8. Catalytic Cycle for Ionic Iodide, Showing Acid-Catalyzed Mechanism for Activation of Methyl Acetate[a]

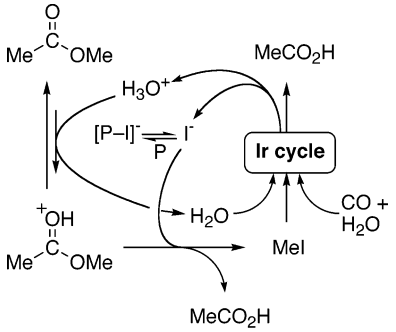

Overall:
$MeOAc + CO + H_2O \rightarrow 2\ MeCO_2H$

$P = Ru(CO)_3I_2$ or InI_3

[a] A similar scheme can also be drawn for activation of methanol.

(expected to be largely dissociated as H_3O^+ and I^-[63]) according to the stoichiometry shown in eq 6.

$$MeI + CO + 2\ H_2O \rightarrow MeCO_2H + H_3O^+ + I^- \quad (6)$$

The onset of catalysis will perturb the standing concentration of $HI_{(aq)}$ above its equilibrium value, explaining the increased proportion of $[Ru(CO)_3I_3]^-$ relative to neutral ruthenium iodocarbonyls. The $HI_{(aq)}$ produced by the Ir cycle must be recycled by reaction with methyl acetate (or methanol) to generate MeI as shown in Scheme 7. We propose that this recycling is accelerated by promoters such as $[Ru(CO)_4I_2]$ or InI_3, thereby moderating the steady state concentration of $HI_{(aq)}$. In the proposed mechanism (Scheme 8) the neutral promoter species $[Ru(CO)_3I_2(sol)]$ or InI_3 scavenges $HI_{(aq)}$ to give $[Ru(CO)_3I_3]^-H_3O^+$ or $InI_4^-H_3O^+$. Crucially the I^- is scavenged into a form in which it no longer acts as a poison for the key migratory insertion reaction (as demonstrated by the model kinetic studies). These species can act as Brønsted acid catalysts for the reaction of $HI_{(aq)}$ with MeOAc, consequently lowering the standing concentration of $HI_{(aq)}$ and enhancing turnover in the Ir cycle. Consistent with this, ^{13}C labeling experiments showed that methyl exchange between MeI and MeOAc is promoted by $[Ru(CO)_3I_3]-H_3O^+$,[64] which can be explained by conventional acid catalysis (eqs 7 and 8).

$$H_3O^+ + MeOC(=O)Me \rightleftharpoons H_2O + [MeOC(OH)Me]^+ \quad (7)$$

$$[MeOC(OH)Me]^+ + I^- \rightleftharpoons MeI + MeCO_2H \quad (8)$$

The presence of a Brønsted acidic H_3O^+ counterion for the anionic promoter species appears to be crucial in obtaining above normal carbonylation rates. This is demonstrated by the observation that the promotional effect of $[Ru(CO)_4I_2]$ is negated by an equimolar quantity of LiI (equivalent to addition of $[Ru(CO)_3I_3]^-Li^+$) (Table S2, Figure 2).[65]

Conclusions

The use of a third-row transition metal in an industrial homogeneous catalytic process is rare; indeed relatively inert 5d metal complexes are often used as models for the more active 3d and 4d congeners. Stronger Ir−ligand bonds and a preference for higher oxidation states lead to important differences in behavior for Ir- and Rh-based methanol carbonylation catalysts. The stronger metal−ligand bonding increases catalyst stability (by reducing susceptibility to CO-loss and precipitationof IrI_3) but has a dramatic inhibitory effect on the migratory CO insertion step of the catalytic cycle. Thus carbonylation of the Ir(III) methyl complex **2** becomes rate determining, and commercially advantageous rates are achieved only using promoters that accelerate this step.

The role of promoters (e.g., transition metal carbonyls/halocarbonyls or group 12/13 iodides) has been investigated in detail. The two different classes of promoter act by a common mechanism. Neutral promoter species (e.g., $[Ru(CO)_3I_2]_2$ or InI_3) are shown to accelerate the stoichiometric carbonylation of the catalyst resting state $[Ir(CO)_2I_3Me]^-$ (**2**) by acting as iodide acceptors (or sources of "iodide holes"). This facilitates conversion of **2** into the neutral tricarbonyl $[Ir(CO)_3I_2Me]$ (**4**), which is carbonylated much faster than the anion, primarily due to increased competition for π-back-donation, which raises the electrophilicity of the carbonyl ligands. In the catalytic process the promoters bind iodide to form a [promoter-I]$^-H_3O^+$ adduct (e.g., $[Ru(CO)_3I_3]^-H_3O^+$ or $InI_4^-H_3O^+$), which catalyzes the reaction of $HI_{(aq)}$ with MeOAc. This moderates the standing concentration of ionic iodide, thereby aiding carbonylation via neutral intermediates. Effective promoters must have a relatively high iodide affinity in order to scavenge iodide into a form in which it no longer acts as a poison for carbonylation.

Experimental Section

Materials. Solvents and reagents were purified by standard methods:[66] Dichloromethane and acetonitrile were distilled from calcium hydride after reflux; diethyl ether was distilled from a purple solution of sodium/benzophenone immediately before use; methanol was distilled from magnesium methoxide (magnesium turnings (1 g), iodine (0.1 g), and spectroscopic grade methanol (200 cm^3), after reflux (24 h)). Other reagents were used as supplied: lithium iodide, methyl acetate, methyl iodide, ^{13}C-methyl iodide, water, Ph_4AsCl, Bu_4NI, InI_3, GaI_3, AlI_3, ZnI_2, $AgBF_4$, I_2, $[Cr(CO)_6]$, $[W(CO)_6]$ (Aldrich), acetic acid (BP Chemicals), iridium and ruthenium chloride hydrates (Johnson Matthey). H_2IrCl_6 was obtained from Johnson Matthey as an aqueous solution and used as supplied. Standard Schlenk techniques and glassware were used for preparative reactions.[67] Nitrogen and carbon monoxide (99.9%, Linde or BOC CP Grade) were dried through a short (20 × 3 cm diameter) column of molecular sieves (4 Å) which was regularly regenerated; the carbon monoxide was also passed through a

(63) The strong acid HI (pK_a ca. −10) will be largely dissociated, according to the equilibrium $HI + H_2O = H_3O^+ + I^-$ in the catalytic medium (aqueous acetic acid).

(64) Scrambling of labeled methyl groups between $^{12}CH_3I$ and $^{13}CH_3OAc$ was monitored by ^1H NMR spectroscopy under conditions (168 °C, aqueous acetic acid, CO, 28.5 barg total pressure) close to those of the catalytic carbonylation system. The extent of $^{13}CH_3$-labeling in MeOAc was determined from the relative intensities of the ^1H singlet of $^{12}CH_3OAc$ and doublet of $^{13}CH_3OAc$ (δ 3.55, $^1J_{CH}$ 147 Hz). Addition of $[Ru(CO)_4I_2]$ (4000 ppm Ru) reduced the half-life for methyl exchange from 144 to 55 min (Supporting Information, Figure S5), representing an acceleration by a factor of 2.6. At the end of the experiment, ^{13}C NMR spectroscopy showed the presence of $[Ru(CO)_4I_2]$ and $[Ru(CO)_3I_3]^-$ in a ca. 1:3 ratio. In studies of Ru/iodide-catalyzed carbonylation and homologation reactions, Braca suggested that "$[Ru(CO)_3I_3]^-H^+$" can activate methyl acetate by protonation: Braca, G.; Sbrana, G.; Valentini, G.; Andrich, G.; Gregorio, G. *J. Am. Chem. Soc.* **1978**, *100*, 6238.

(65) Conversely, ruthenium can negate the poisoning effect of LiI by scavenging I^- to give $[Ru(CO)_3I_3]^+Li^+$.

(66) Perrin, D. D.; Armerego, W. L. F.; Perrin, D. R. *Purification of Laboratory Chemicals*, 3rd ed.; Pergamon Press: Oxford, 1988.

(67) Shriver, D. F. *The Manipulation of Air Sensitive Compounds*; McGraw-Hill: New York, 1986.

short column of activated charcoal to remove any iron pentacarbonyl impurity.[68] Bulbs of ^{13}C-enriched carbon monoxide for preparative labeling of complexes were supplied by Cambridge Isotope Laboratories and Aldrich. High-pressure ^{13}CO for HPNMR experiments was supplied by Isotec Inc. [$Ru_3(CO)_{12}$] was supplied by Strem or prepared from ruthenium chloride by the method of Bruce et al.[69] Salts of [$Ru(CO)_3I_3]^-$ and [$Ru(CO)_2I_4]^{2-}$ were prepared by established methods.[70]

Instrumentation. Routine IR spectra were recorded on either a Perkin-Elmer 1640, a Perkin-Elmer 1710, or a Mattson Genesis Fourier transform spectrometer using a solution cell with CaF_2 windows (path length 0.1 or 0.5 mm). High-pressure/high-temperature IR spectra were recorded on a Perkin-Elmer 1710 Fourier transform spectrometer using a SpectraTech cylindrical internal reflectance (CIR) cell (vide infra). ^{1}H spectra were recorded on either a Bruker AM250 or a Bruker AC250 instrument with a Bruker B-ACS60 automatic sample changer operating in pulse Fourier transform mode using the solvent as reference. ^{13}C NMR spectra were recorded on either a Bruker WH400 or a Bruker AMX 400 Fourier transform instrument, again with solvent as the internal standard. High-pressure NMR spectra (^{1}H and ^{13}C) were measured on a JEOL 400 MHz NMR spectrometer at the BP Chemicals Research Centre in Sunbury-on-Thames (UK) using sapphire tubes (5 mm o.d.) supplied by Saphikon, pressure rated to 160 barg, fitted (cemented) with a titanium valve. Osmometry measurements were made using a Wescar 5500 vapor pressure osmometer, calibrated using benzil solutions of known concentration in the required solvent. Elemental analyses were determined by the University of Sheffield microanalysis service.

Synthesis of Iridium Complexes. (a) $Ph_4As[Ir(CO)_2I_2]$, 1. This compound was prepared by a variation of the method described by Forster.[71] $IrCl_3 \cdot xH_2O$ (1.64 g, 4.65 mmol, assuming $x = 3$) and NaI (10 g, large excess) were dissolved in a mixture of 2-methoxyethanol (80 cm^3) and distilled water (5 cm^3) and refluxed, while a stream of carbon monoxide was bubbled through the solution. Over the course of 6 h the black solution turned pale yellow. Ph_4AsCl (2.2 g, 5.3 mmol), dissolved in 2-methoxyethanol (5 cm^3), was added to the hot solution, which was then filtered through Celite. Distilled water was added to the solution until the precipitation of $Ph_4As[Ir(CO)_2I_2]$ commenced. The precipitation was allowed to go to completion at −20 °C under an atmosphere of carbon monoxide. The bright yellow precipitate was filtered, washed with cold methanol then diethyl ether, and dried in vacuo; yield 3.42 g (70%). Anal. Calcd for ($C_{26}H_{20}AsI_2IrO_2$): C, 35.3; H, 2.3; I, 28.7. Found: C, 35.1; H, 2.3; I, 28.4. IR (CH_2Cl_2) ν(CO)/cm^{-1}: 2046, 1968. ^{13}C NMR ($CDCl_3$): δ 169.7 (*C*O) 134.8, 132.8, 131.5 (Ph, *C*H) 120.1 (Ph, As*C*). An analogous procedure was used to prepare $Bu_4N[Ir(CO)_2I_2]$, using Bu_4NI in place of Ph_4AsCl.

(b) $Ph_4As[Ir(^{13}CO)_2I_2]$. $Ph_4As[Ir(CO)_2I_2]$ (400 mg, 4.5×10^{-4} mol) was dissolved in CH_2Cl_2 (40 cm^3) in a two-necked round-bottomed flask under N_2 which was connected to a high-vacuum line fitted with a Toepler pump and a 1 dm^3 bulb of ^{13}C-labeled carbon monoxide. The flask was evacuated and then opened to admit ^{13}CO while stirring the solution at the gas−liquid interface. At regular intervals the gas above the solution was exchanged with fresh ^{13}CO from the bulb and a sample of the solution was removed by syringe for analysis by IR spectroscopy. This was continued until the solution was approximately 95% ^{13}CO labeled, as judged by the IR spectrum. The ^{13}CO in the reaction flask was transferred back to the reservoir bulb using the Toepler pump before removing the reaction flask. The solvent was removed and the product washed with diethyl ether and dried in vacuo. IR (CH_2Cl_2) ν(CO)/cm^{-1}: 1997, 1923. ^{13}C NMR ($CDCl_3$): δ 169.8 (*C*O) 134.9, 133.0, 131.5 (Ph, *C*H) 120.2 (Ph, As*C*).

(c) $Ph_4As[Ir(CO)_2I_3Me]$, 2. $Ph_4As[Ir(CO)_2I_2]$ (1 g, 1.1 mmol) was dissolved in methyl iodide (10 cm^3) and stirred under nitrogen for 1 h. The methyl iodide was removed in vacuo. Recrystallization from CH_2Cl_2−Et_2O gave orange crystals, which were dried in vacuo, yield 1.08 g (93%). Anal. Calcd for ($C_{27}H_{23}AsI_3IrO_2$): C, 31.6; H, 2.3; I, 37.1. Found: C, 31.8; H, 2.4; I, 37.0. IR (CH_2Cl_2) ν(CO)/cm^{-1}: 2098, 2046. ^{1}H NMR ($CDCl_3$): δ 2.1 (s, 3H, C*H*$_3$), 7.6−7.9 (m, 20H, Ph_4As). ^{13}C NMR ($CDCl_3$): δ 155.5 (*C*O) 134.9, 132.9, 131.5 (Ph, *C*H) 120.2 (Ph, As*C*); −16.3 (*C*H$_3$). An analogous procedure was used to prepare $Bu_4N[Ir(CO)_2I_3Me]$. ^{13}CO-labeled $Ph_4As[Ir(^{13}CO)_2I_3Me]$ was prepared by the same method using $Ph_4As[Ir(^{13}CO)_2I_2]$ as the precursor. IR (CH_2Cl_2) ν(CO)/cm^{-1}: 2049, 1998. ^{13}CH$_3$-labeled $Ph_4As[Ir(CO)_2I_3(^{13}CH_3)]$ was prepared by the same method using $^{13}CH_3I$. ^{1}H NMR ($CDCl_3$): δ 2.1 (d, 3H, C*H*$_3$ $^1J_{H-C}$ 139 Hz). The doubly labeled compound $Ph_4As[Ir(^{13}CO)_2I_3(^{13}CH_3)]$ was prepared by the same method from $Ph_4As[Ir(^{13}CO)_2I_2]$ and $^{13}CH_3I$. ^{13}C NMR ($CDCl_3$): δ 155.5 (d *C*O), −16.3 (t, *C*H$_3$) $^2J_{C-C}$ 1.2 Hz.

(d) $[Ir(CO)_2I_2Me]_2$, 3d. Anhydrous InI_3 (350 mg, 0.706 mmol) was added to a stirred solution of $Bu_4N[Ir(CO)_2I_3Me]$ (500 mg, 0.564 mmol) in CH_2Cl_2 (20 cm^3) under nitrogen (20 °C). Stirring was continued (1 h) while an orange powder started to precipitate. The solvent was removed in vacuo to leave an orange-red solid residue from which pure $[Ir(CO)_2I_2Me]$ was extracted into hot cyclohexane by adding portions of 20 cm^3 until the solution remained colorless. The combined extracts were evaporated to dryness, and the product was obtained as an orange powder, yield 220 mg, 75%. Anal. Calcd for ($C_6H_6I_4Ir_2O_4$): C, 7.0; H, 0.6; I, 49.1. Found: C, 7.0; H, 0.4; I, 49.1. MW: calcd 1034, found 1001 (PhCl); 538 (MeCN). IR (CH_2Cl_2) ν(CO)/cm^{-1}: 2119, 2074. ^{1}H NMR (CD_2Cl_2): δ 1.94 (major), 1.88 (minor) (C*H*$_3$, 2 isomers in ratio ca. 5:2). ^{13}C NMR (CD_2Cl_2): δ 152.4, 150.3, 150.0 (*C*O) −5.30, −8.76 (*C*H$_3$). Recrystallization from hot chloroform gave crystals suitable for a single-crystal X-ray structure determination.

(e) $Ph_4As[Ir(CO)_2I_3(COMe)]$, 6. $Ph_4As[Ir(CO)_2I_3Me]$ (0.380 g, 0.375 mmol) was dissolved in THF (20 cm^3). MeOH (0.5 cm^3) and MeI (0.1 cm^3) were added, and the solution was transferred to a Fisher-Porter apparatus. The vessel was flushed twice with CO (5 barg), then pressurized with CO to 10 barg, and warmed to 40 °C using an oil bath. After stirring for 3 days the CO was released and the solution transferred to a Schlenk tube and evaporated to dryness in vacuo. The crude product was recrystallized by dissolving in CH_2Cl_2 (5 cm^3), layering with Et_2O, and cooling to 5 °C to give yellow-orange crystals. A suitable crystal was selected for X-ray diffraction. The remaining crystals were separated from the solution and dried in vacuo, yield 0.299 g (76%). Anal. Calcd for ($C_{28}H_{23}AsI_3IrO_3$): C, 31.87; H, 2.20. Found: C, 31.97; H, 2.05. IR (CH_2Cl_2) ν(CO)/cm^{-1}: 2110, 2062, 1697, 1658. ^{1}H NMR (CD_2Cl_2): δ 2.94, 2.67 (each s, total 3H, COC*H*$_3$ for **6a** and **6b** in ratio ca. 9:1), 7.6−7.9 (m, 20H, Ph_4As). ^{13}C NMR (CD_2Cl_2): δ 196.42, 198.06 (*C*OMe, **6a** and **6b**, respectively), 151.96, 160.84 (Ir-*C*O, **6a** and **6b**, respectively), 131.62, 133.27, 135.18 (Ph, *C*H), 120.64 (Ph, *C*-As), 49.88, 50.91 (CO*C*H$_3$, **6a** and **6b**, respectively).

Synthesis of Ruthenium Complexes. (a) $[Ru(CO)_4I_2]$. Method 1. Acetic acid (204.0 g, 3.40 mol), iodine (12.20 g, 48.1 mmol), and [$Ru_3(CO)_{12}$] (9.99 g, 15.6 mmol) were placed in a 300 mL zirconium autoclave (Parr), and the autoclave was sealed. The autoclave was pressure tested with nitrogen (30 barg) and then vented. The autoclave was flushed three times with CO (10 barg) and pressurized with CO to 10 barg. The contents were then heated to 180 °C with stirring (1500 rpm). Once at temperature the total reactor pressure was increased to 25 barg by feeding CO to the autoclave. The reactor was held at temperature for 1 h and then cooled. On opening the autoclave, an orange precipitate was found to be present in the solution, on the reactor base, and around the autoclave walls and stirrer shaft. This precipitate was removed by filtration to give a bright orange solution. Water (ca. 700 cm^3) was added to the filtrate to precipitate an orange powder. The orange solid was filtered off and washed with water (5 × 50 cm^3) and then dried in vacuo to yield [$Ru(CO)_4I_2$] (14.0 g, 64% yield). IR (CH_2Cl_2) ν(CO)/cm^{-1}: 2165, 2109, 2094sh, 2076.

(68) Haynes, A.; Ellis, P. R.; Byers, P. K.; Maitlis, P. M. *Chem. Br.* **1992**, *28*, 517.
(69) Bruce, M. I.; Jensen, C. M.; Jones, N. L. *Inorg. Synth.* **1990**, *28*, 216.
(70) Colton, R.; Farthing, R. H. *Aust. J. Chem.* **1971**, *24*, 903.
(71) Forster, D. *Inorg. Nucl. Chem. Lett.* **1969**, *5*, 433.

Method 2. A variation of the method used by Johnson[72] was also used. Heptane solutions of $Ru_3(CO)_{12}$ (100 mg, 1.56 mmol in 100 cm^3) and iodine (127 mg, 0.50 mmol in 100 cm^3) were cooled (−40 °C) using a solid carbon dioxide−acetone bath, before mixing to give immediate formation of a brown suspension, which became more dense as the solution was allowed to warm to room temperature. The heptane was removed in vacuo to leave a brown powder, which exhibited an IR spectrum consistent with a mixture of $[Ru(CO)_4I_2]$ and $[Ru(CO)_3I_2]_2$. A sample (100 mg) of the mixture produced by this method was dissolved in CH_2Cl_2 (15 cm^3). The solution was transferred to a Fisher-Porter tube, pressurized with CO (10 barg), and heated to 40 °C. After one week the infrared spectrum of the solution indicated the sole presence of $[Ru(CO)_4I_2]$. Removal of the CH_2Cl_2 by bubbling CO through the solution to dryness left $[Ru(CO)_4I_2]$ as a yellow powder. IR ν(CO)/cm^{-1} (CH_2Cl_2): 2161, 2106, 2097, 2068.

(b) $[Ru(CO)_3I_2]_2$. A sample (300 mg) of the mixture produced in (a) method 2 was dissolved in $CHCl_3$ (15 cm^3), and the solution was refluxed under N_2 for 3 h, at which point the IR spectrum indicated the sole presence of $[Ru(CO)_3I_2]_2$. The solvent was removed in vacuo to leave $[Ru(CO)_3I_2]_2$ as a red-brown powder. IR ν(CO)/cm^{-1} (CH_2Cl_2): 2123, 2067.

(c) $[Ru(CO)_2I_2]_n$. This compound was prepared by a variation of the method described by Johnson.[72] $Ru_3(CO)_{12}$ (100 mg, 1.56 mmol) and iodine (127 mg, 0.5 mmol) were added to *n*-nonane (50 cm^3) and refluxed under N_2 for 3 h. The resultant brown suspension was cooled and filtered to give a rust-brown product. Yield: 148 mg (77%). IR ν(CO)/cm^{-1} (*n*-nonane): 2060, 2000.

Synthesis of Ph_4AsI. Ph_4AsCl (1.00 g, 2.39 mmol) and NaI (3 g, 20 mmol) were dissolved in methanol (50 cm^3) in a round-bottom flask and stirred (16 h). The solvent was removed in vacuo and the resulting white solid dissolved in dichloromethane and filtered through Celite to remove excess NaI. The solvent was removed under vacuum and the solid recrystallized from CH_2Cl_2−Et_2O, yield 1.01 g, 83%. Anal. Calcd for ($C_{24}H_{20}AsI$): C, 56.5; H, 3.95; I, 24.9. Found: C, 56.4; H,3.99; I, 25.0.

X-ray Structure Determination for 6a. Data were collected on a Bruker Smart CCD area detector with an Oxford Cryostream 600 low-temperature system using Mo Kα radiation ($\bar{\lambda}$ = 0.71073 Å). The structure was solved by direct methods and refined by full matrix least-squares methods on F^2. Hydrogen atoms were placed geometrically and refined using a riding model (including torsional freedom for methyl groups). Complex scattering factors were taken from the SHELXL program packages.[73] Crystallographic data are summarized in Table 4, and full listings are given in the Supporting Information.

Batch Carbonylation Experiments. Carbonylation experiments were performed using a 300 mL zirconium autoclave (Parr) equipped with a magnetically driven stirrer, liquid injection facility, and water fed cooling coils. A carbon monoxide supply to the autoclave was provided from a ballast vessel, feed gas being provided on demand to maintain the autoclave at a constant pressure. The rate of carbon monoxide consumption was used to calculate the carbonylation rate (in mol dm^{-3} h^{-1}) at 50% conversion of methyl acetate, the consumption of 1 mol of carbon monoxide, 1 mol of methyl acetate, and 1 mol of water being equivalent to the carbonylation of 1 mol of methanol. For each batch carbonylation experiment the catalyst, H_2IrCl_6, dissolved in a portion of an acetic acid−water mixture (7.5 g each) was charged to the liquid injection facility. If an additive was used, this was placed in the reactor and covered with a portion of the acetic acid charge (10 g), and the reactor was sealed. The reactor was then pressure tested with nitrogen and vented. The autoclave was then flushed with carbon monoxide several times. The remaining liquid components of the reaction composition were charged to the autoclave via a liquid addition port. The autoclave was flushed with CO, pressurized with carbon monoxide (ca. 5 barg), and heated with stirring (1500 rpm) to the reaction temperature. The total pressure was then raised to approximately 3 bar below the desired operating pressure by feeding carbon monoxide from the ballast vessel. Once stable at temperature, the catalyst was injected using an overpressure of carbon monoxide to achieve the required pressure. The reactor pressure was maintained constant (±0.5 bar) by feeding gas from the ballast vessel throughout the experiment. Gas uptake from the ballast vessel was measured using data-logging facilities throughout the course of the experiment. The reaction temperature was maintained within ±1 °C of the desired reaction temperature by means of a heating mantle connected to a Eurotherm control system. In addition, excess heat of reaction was removed by means of the cooling coils. At the end of the reaction the ballast vessel was isolated and the reactor crash-cooled by use of the cooling coils.

Table 4. Summary of Crystallographic Data for **6a**[Ph_4As]

formula	$C_{28}H_{23}AsI_3O_3Ir$
fw	1055.28
cryst syst	monoclinic
space group	$P2_1/n$
color	yellow
a (Å)	12.351(3)
b (Å)	16.500(4)
c (Å)	15.971(4)
α (deg)	90
β (deg)	110.277(4)
γ (deg)	90
temp (K)	100(2)
Z	4
final *R* indices [I>2σ(I)]	R1 = 0.0325
	wR2 = 0.0770
R indices (all data)	R1 = 0.0434
	wR2 = 0.0809
GOF	1.007

In Situ IR Spectroscopic Monitoring of Catalytic Reactions. Catalytic reactions were monitored in situ by high-pressure IR spectroscopy using a modified batch autoclave in which all wetted parts were manufactured from Hastelloy B2. An autoclave head unit comprising a Magnedrive stirrer, a pressure gauge, two liquid feed lines, a gas feed line, and a thermocouple well was placed on a 300 cm^3 base fitted with an ASI Systems Inc. Sentinel SiComp ATR probe. The unit was sealed before transferring to a blast bay. An electrical band heater and thermocouple were placed on the autoclave assembly before connecting to the gas and liquid feed lines, water cooling hoses, and overhead stirrer. The Sentinel probe was connected to an ASI systems ReactIR 1000 series spectrometer via an optical conduit. The gas and liquid feed inlet valves were opened, and the assembly pressure was tested with nitrogen (32 barg). The unit was flushed with nitrogen (2 × 20 barg pressure and vent cycles). The Sentinel probe was aligned and a background spectrum taken before flushing the autoclave unit with carbon monoxide (3 × 10 barg pressure and vent cycles). The autoclave was opened to vent and a funnel connected to the liquid inlet. Methyl iodide followed by the remainder of the autoclave charge (including any additives) was added via the funnel before removing it and resealing the autoclave. The iridium catalyst solution was placed into the catalyst injector followed by an acetic acid wash. The autoclave stirrer was switched on before pressurizing with carbon monoxide (6 barg). The assembly was heated to reaction temperature (190 °C). Once the temperature had stabilized, the pressure in the autoclave was adjusted to the desired initial pressure (19 barg) as was the catalyst injector (34 barg). The ballast vessel was charged with carbon monoxide (54 barg) before injecting the catalyst solution. After injection the autoclave was adjusted to the desired pressure (22 barg), which was kept constant by feeding carbon monoxide from the ballast vessel on demand. The temperature in the autoclave was kept constant by

(72) Johnson, B. F. G.; Johnson, R. D.; Lewis, J. *J. Chem. Soc. (A)* **1969**, 792.
(73) Sheldrick, G. M. *SHELXL93*, An integrated system for solving and refining crystal structures from diffraction data; University of Gottingen: Germany, 1993. Sheldrick, G. M. *SHELXL97*, An integrated system for solving and refining crystal structures from diffraction data; University of Gottingen: Germany, 1997.

controlling the flow of cooling water. Spectra were recorded automatically by the ReactIr system. Spectra were recorded by accumulating 128 scans at a resolution of 4 cm^{-1} every 60−90 s. On completion of the run, the ballast vessel was isolated, the heating switched off, and the autoclave crash-cooled to below 30 °C. Once below 30 °C, the autoclave was removed from the bay, emptied, and cleaned. Analogous results were also obtained using a transmission HPIR cell, based on a modified batch autoclave equipped with CaF_2 windows (path length 0.1 mm) and fitted with an electromagnetic agitator, gas feeds, and a catalyst injection system. In this case spectra were recorded using a Nicolet 710 spectrometer with a KBr beam splitter and MCT detector.

In Situ IR Spectroscopic Monitoring of Model Reactions. Model reactions were monitored in situ by high-pressure IR spectroscopy using a cylindrical internal reflectance (CIR) cell comprising a batch autoclave (Parr) modified (by SpectraTech) to accommodate a crystalline silicon CIR rod as described by Moser.[74] Spectra were recorded using a Perkin-Elmer 1710 FTIR spectrometer fitted with an MCT detector. The cell was placed either in an external optical bench coupled to the spectrometer or directly in the spectrometer sample compartment. The reaction solution was prepared by dissolving the iridium compound $Ph_4As[Ir(CO)_2I_3Me]$ (typically 0.3 g, 0.29 mmol) or $[Ir(CO)_2I_2Me]_2$ (typically 0.15 g, 0.145 mmol or 0.29 mmol Ir) and the appropriate amount of any additive (see Tables S4−S7) in the required solvent (8 cm^3). The reaction solution was then filtered into the CIR cell. The cell head was fitted to the body of the cell, ensuring that the stirrer was firmly tightened into the cell head. The vent lines, stirrer, and gas inlet from the cylinder were then fitted, tightened as required, and flushed out four times with the gas to be used in the experiment, typically carbon monoxide. The cell was then flushed with the same gas at least four times, the last two with the stirrer on, and then slowly filled to the required pressure. The cell was then heated to the required reaction temperature, and spectra were recorded over the range 2200−1600 cm^{-1} at regular intervals under computer control. Data analysis was achieved using the Kaleidagraph package to obtain pseudo-first-order rate constants by fitting exponential curves to absorbance vs time data. All reaction rates were reproducible to ±5%. The values quoted are averages of all the runs performed.

Computational Details. Ab initio quantum mechanical calculations using second-order Møller−Plesset (MP2) theory were performed using the Gaussian94 suite of programs.[75] Geometries of stationary points were optimized using the Berny algorithm[76] as implemented in Gaussian94. Transition states were located by employing a reaction coordinate method followed by a transition state search based on the Berny algorithm and characterized by frequency calculations to give Hessians with a single negative eigenvalue. We employed the LANL2DZ (abbreviated as 2DZ) Gaussian basis set developed by Hay and Wadt,[77] which uses a semi-core double-ζ contraction scheme for the heavy elements Ir, Ru, Rh, I, and In, with the light atoms C, O, and H being described by the split-valence Dunning 9-5V all-electron basis. To obtain more accurate energy estimates, an extended LANL2DZ* basis set was used, either in a single-point calculation at the 2DZ optimized geometry or in a full optimization. The 2DZ* basis was generated by the addition of a single high angular momentum polarization function to the 2DZ basis of each atom. The orbital exponents of polarization functions used in the 2DZ* basis were 1.100 (p) for H,[75] 1.154 (d) for O,[78] 0.600 (d) for C,[78] 0.250 (d) for I,[79] and 1.000 (arbitrary) (d) for Ir, Ru, and Rh. Solvent effects were considered using the polarizable continuum model (PCM).[80]

Acknowledgment. This work was supported by BP Chemicals Ltd (PDRF to T.G., CASE studentships to P.W.B., C.M.B., P.I.P.E., T.R.G., J.M.P., P.W.V.), the University of Sheffield, The Royal Society, and EPSRC. An award of ^{13}CO was made by Cambridge Isotope Laboratories. Dr. A. Castro is thanked for assistance with X-ray crystallography and Dr. S. Haak for the results in ref 62.

Supporting Information Available: Tables of kinetic data for catalytic and stoichiometric reactions. In situ HPIR spectra. Tables of X-ray crystallographic data for **3d** and **6a**. Atomic coordinates for optimized structures and selected reaction energetics data from ab initio calculations. This material is available free of charge via the Internet at http://pubs.acs.org.

JA039464Y

(74) Moser, W. R. In *Homogeneous Transition Metal Catalysed Reactions*; Moser, W. R., Slocum, D. W., Eds.; Advances in Chemistry Series, Vol. 230, American Chemical Society: Washington, DC, 1992; pp 3−18.

(75) Frisch, M. J.; Trucks, G. W.; Schlegel, H. B.; Gill, P. M. W.; Johnson, B. G.; Robb, M. A.; Cheeseman, J. R.; Keith, T.; Petersson, G. A.; Montgomery, J. A.; Raghavachari, K.; Al-Laham, M. A.; Zakrzewski, V. G.; Ortiz, J. V.; Foresman, J. B.; Cioslowski, J.; Stefanov, B. B.; Nanayakkara, A.; Challacombe, M.; Peng, C. Y.; Ayala, P. Y.; Chen, W.; Wong, M. W.; Andres, J. L.; Replogle, E. S.; Gomperts, R.; Martin, R. L.; Fox, D. J.; Binkley, J. S.; Defrees, D. J.; Baker, J.; Stewart, J. P.; Head-Gordon, M.; Gonzalez, C.; Pople, J. A. *Gaussian 94* (Revision D.4); Gaussian, Inc.: Pittsburgh, PA, 1995.

(76) Schlegel, H. B. *J. Comput. Chem.* **1982**, *3*, 214.

(77) Hay, P. J.; Wadt, W. R. *J. Chem. Phys.* **1985**, *82*, 270. Wadt, W. R.; Hay, P. J. *J. Chem. Phys.* **1985**, *82*, 284. Hay, P. J.; Wadt, W. R. *J. Chem. Phys.* **1985**, *82*, 299.

(78) Huzinaga, S.; Andzelm, J.; Klobukowski, M.; Radzio-Andzelm, E.; Sakai, Y.; Tatewaki, H. *Gaussian Basis Sets for Molecular Calculations*; Physical Sciences Data Vol. 16; Elsevier: Amsterdam, 1984.

(79) The exponent value for iodine is intermediate between the values given in ref 78 for I and I^-.

(80) Miertus, S.; Scrocco, E.; Tomasi, J. *J. Chem. Phys.* **1981**, *55*, 117. Miertus, S.; Tomasi, J. *Chem. Phys.* **1982**, *65*, 239.